

On CSI-free Multi-Antenna Schemes for Massive Wireless Energy Transfer

Onel L. A. López, Samuel Montejo-Sánchez, Richard D. Souza, Hirley Alves, Constantinos B. Papadias

Abstract—Wireless Energy Transfer (WET) is emerging as a potential green enabler for massive Internet of Things (IoT). Herein, we analyze Channel State Information (CSI)-free multi-antenna strategies for powering wirelessly a large set of single-antenna IoT devices. The CSI-free schemes are AA – SS (AA – IS), where all antennas transmit the same (independent) signal(s), and SA, where just one antenna transmits at a time such that all antennas are utilized during the coherence block. We characterize the distribution of the provided energy under correlated Rician fading for each scheme and find out that while AA – IS and SA cannot take advantage of the multiple antennas to improve the average provided energy, its dispersion can be significantly reduced. Meanwhile, AA – SS provides the greatest average energy, but also the greatest energy dispersion, and the gains depend critically on the mean phase shifts between the antenna elements. We find that consecutive antennas must be π phase-shifted for optimum average energy performance under AA – SS. Our numerical results evidenced that correlation is beneficial under AA – SS, while a greater line of sight (LOS) and/or number of antennas is not always beneficial under such scheme. Meanwhile, both AA – IS and SA schemes benefit from small correlation, large LOS and/or large number of antennas.

Index Terms—massive WET, IoT, CSI-free, Rician fading, phase shifts

I. INTRODUCTION

Internet of Things (IoT), where every *thing* is practically transformed into an information source, represents a major technology trend that is revolutionizing the way we interact with our surrounding environment so that we can make the most of it. There are two general categories of IoT use cases [1]: i) critical IoT, with stringent requirements on reliability, availability, and low latency, e.g. in remote health care, traffic safety and control, industrial applications and control, remote manufacturing, surgery; and ii) massive IoT, where sensors

Onel L. A. López and Hirley Alves are with the Centre for Wireless Communications (CWC), University of Oulu, Finland. {onel.alcarazlopez,hirley.alves}@oulu.fi

S. Montejo-Sánchez is with Programa Institucional de Fomento a la I+D+i, Universidad Tecnológica Metropolitana, Santiago, Chile. {smontejo@utem.cl}.

Richard D. Souza is with Federal University of Santa Catarina (UFSC), Florianópolis, Brazil. {richard.demo@ufsc.br}.

Constantinos B. Papadias is with Broadband Wireless & Sensor Networks Research Lab, Athens Information Technology, Athens 15125, Greece. {papadias@ait.edu.gr}.

This work is supported by Academy of Finland (Aka) (Grants n.307492, n.318927 (6Genesis Flagship), n.319008 (EE-IoT)), as well as Finnish Foundation for Technology Promotion, FONDECYT Postdoctoral Grant n.3170021 in Chile, the National Council for Scientific and Technological Development (CONICYT) and by project Print CAPES-UFSC “Automation 4.0” in Brazil.

This work has been submitted to the IEEE for possible publication. Copyright may be transferred without notice, after which this version may no longer be accessible.

typically report to the cloud, and the requirement is for low-cost devices with low energy consumption and good coverage. In such massive deployments, these IoT nodes are not generally supposed to be transmitting continuously, but they do require to operate for long periods of time without batteries replacement, specially since many of them could be placed in hazardous environments, building structures or the human body. One important enabler under consideration is Wireless Energy Transfer (WET), so IoT nodes would be equipped with an energy harvesting (EH) circuitry that allows them to harvest energy from incoming radio frequency (RF) signals [2].

WET holds vast potential for replacing batteries or increasing their lifespans. In fact, RF-EH devices can become self-sustaining with respect to the energy required for operation, thereby obtaining an unlimited operating lifespan while demanding negligible maintenance [3]. This is crucial for the future society since the processing of battery wastes is already a critical problem. The most effective approach for reducing battery wastes is to avoid using them, for which WET is an attractive clean solution. Notice that with the continuous advances on circuitry technology aiming at reducing further the power consumption of low-cost devices¹, e.g. printed sensors technology [6], it is expected an exponential growth on WET-enabled IoT applications.

The IoT paradigm intrinsically includes wireless information transfer (WIT), thus WET appears naturally combined with WIT. In such case two main architectures can be distinguished in literature: i) Wireless Powered Communication Network (WPCN), where WET occurs in the downlink in a first phase and WIT takes place in the second phase; and ii) Simultaneous Wireless Information and Power Transfer (SWIPT), where WET and WIT occur simultaneously. Readers can refer to [7] to review the recent progress on both architectures, while herein the discussions will focus merely on WPCN and pure WET setups. Notice that in most of practical applications WET duration would be significantly larger than WIT in order to harvest usable amounts of energy [2]. Actually, some use cases require operating under WET almost permanently while WIT happens sporadically, e.g. due to event-driven traffic. Therefore, enabling efficient WET is

¹Currently there is available a wide-range of IoT devices that seem suitable for relying on a RF-EH module as the main power supply due to their extremely low power consumption profiles. For instance, accelerometer ADXL362 ($\sim 40\mu\text{W}$ in active) and Light ISL29033 ($\sim 100\mu\text{W}$ in active) [4]. In fact, the first wireless battery-free bio-signal processing system on chip was introduced by [5] and it is able to monitor various bio-signals via electrocardiogram, electromyogram, and electroencephalogram. The total size of the chip is 8.25mm^2 and consumes $19\mu\text{W}$ to measure heart rate.

mandatory for realizing the IoT paradigm and constitutes the scope of this work.

A. Related Work

Recent works have specifically considered WET and WPCN setups in different contexts and scenarios. Key networking structures and performance enhancing techniques to build an efficient WPCN are discussed in [8], where authors also point out challenging research directions. Departing from the simple Harvest-then-Transmit (HTT) scheme [9]–[11] several other protocols have been proposed over the past few years to boost the WPCN performance such as the Harvest-then-Cooperate (HTC) system studied in [12]–[14] and the power control scheme relying on energy accumulation between transmission rounds discussed in [15]. Authors either analyze the performance of the information transmission phase, or optimize it by using power control or cooperative schemes. Some scheduling strategies that allow a direct optimization of the energy efficiency of the network are also proposed in [16]. Additionally, an energy cooperation scheme that enables energy cooperation in battery-free wireless networks with WET is presented in [17]. Meanwhile, the deployment of single-antenna power beacons (PBs) for powering the mobiles in an uplink cellular network is proposed in [18]. Therein, authors investigate the network performance under an outage constraint on data links using stochastic-geometry tools, while they corroborate the effectiveness of relying on directed WET instead of using isotropic antennas.

Yet, shifts in the system architecture and in the resource allocation strategies for optimizing the energy supply to massive IoT deployments are still required. In [2] we discuss several techniques that seem suitable for enabling WET as an efficient solution for powering the future IoT networks. They are

- **Energy beamforming (EB)**, which allows the energy signals at different antennas to be carefully weighted to achieve constructive superposition at intended receivers. The larger the number of antennas installed at the PB, the sharper the energy beams can be generated in some particular spatial directions. The EB benefits for WPCNs have been investigated for instance in [19] in terms of average throughput performance, while in [20] authors propose an EB scheme that maximizes the weighted sum of the harvested energy and the information rate in a multiple-input single-output (MISO) system. However, the benefits of EB in practice depend on the available CSI at the transmitter, and although there has been some works proposing adequate channel acquisition methods, e.g. [21], [22], this still constitutes a serious limitation. This is due to the harsh requirements in terms of energy and scheduling policies, which become even more critical as the number of EH devices increases;
- **Distributed Antenna Systems (DAS)**, which are capable of eliminating blind spots while homogenizing the energy provided to a given area and supporting ubiquitous energy accessibility. The placement optimization of single-antenna energy and information access points in WPCNs is investigated in [23], where authors focus on minimizing the network deployment cost subject to energy

harvesting and communication performance constraints. On the other hand, authors in [24] study the probability density function (PDF), the cumulative distribution function (CDF), and the average of the energy harvested in DAS, while they determine appropriate strategies when operating under different channel conditions by using such information. Although works in this regard have avoided the use of multiple transmit antennas, we would like to highlight the fact that multiple separate PBs, each equipped with multiple transmit antennas, could alleviate the issue of CSI acquisition when forming efficient energy beams in multiple-users setups, since each PB may be responsible for the CSI acquisition procedure of a smaller set of EH devices;

- **CSI-limited/CSI-free schemes.** Even without accounting for the considerable energy resources demanded by CSI acquisition, the performance of CSI-based systems decays quickly as the number of served devices increases. Therefore, in massive deployment scenarios the broadcast nature of wireless transmissions should be intelligently exploited for powering simultaneously a massive number of IoT devices with minimum or non CSI. Very recently, and for the first time, we proposed in [25] several CSI-free multi-antenna schemes that a PB could utilize to power efficiently a large set of nearby EH devices, while we analyzed their performance in Rician correlated fading channels. We found out that i) the switching antenna (SA) strategy, where a single antenna with full power transmits at a time, provides the most predictable energy source, and it is particularly suitable for powering sensor nodes with highly sensitive EH hardware operating under non line of sight (NLOS) conditions; and ii) transmitting simultaneously the same signal with equal power in all antennas (AA, but herein referred as AA – SS) is the most beneficial scheme when LOS increases and it is the only scheme that benefits from spatial correlation. However, the performance analysis was carried out under the idealistic assumption of channels sharing the same mean phase.

B. Contributions and Organization of the Paper

This paper builds on CSI-free WET with multiple transmit antennas to power efficiently a large set of IoT devices. Different from our early work in [25], herein we do consider the mean phase shifts between antenna elements, which is a practical and unavoidable phenomenon. Based on such modeling we arrive to conclusions that are similar in some cases but different in others to those in [25]. Specifically, the main contributions of this work can be listed as follows:

- We analyze the CSI-free multi-antenna strategies proposed in [25], e.g. AA – SS and SA, in addition to a new scheme named *All Antennas transmitting Independent Signals* (AA – IS), but under shifted mean phase channels. We do not consider any other information related to devices such as topological deployment, battery charge; although, such information could be crucial in some setups. Our derivations are specifically relevant for

- scenarios where it is difficult and/or not worth obtaining such information, e.g. when powering a massive number of low-power EH devices uniformly distributed in a given area and possibly with null/limited feedback to the PB;
- By considering the non-linearity of the EH receiver we demonstrated that those devices far from the PB and more likely to operate near their sensitivity level, benefit more from the SA scheme than from AA – IS. However, those closer to the PB and more likely to operate near saturation, benefit more from AA – IS;
 - We attain the distribution and some main statistics of the RF energy at the EH receiver in correlated Rician fading channels under each WET scheme. Notice that the Rician fading assumption is general enough to include a class of channels, ranging from Rayleigh fading channel without LOS to a fully deterministic LOS channel, by varying the Rician factor κ ;
 - While AA – IS and SA cannot take advantage of the multiple antennas to improve the average statistics of the incident RF power, the energy dispersion can be significantly reduced, hence, reducing the chances of energy outage. Meanwhile, the gains attained by AA – SS in terms of average RF energy delivery depend critically on the mean phase shifts between the antenna elements. In that regard, we show the considerable performance gaps between the idealistic AA – SS proposed in [25] and such scheme when considering channels with different mean phases. Even under such performance degradation AA – SS still provides the greatest average harvested energy when compared to AA – IS and SA, although its associated energy outage probability is generally the worst;
 - We attained the optimum preventive phase shifting for maximizing the average energy delivery or minimizing its dispersion for each of the schemes. We found that when transmitting the same signal simultaneously over all the antennas (AA – SS, or equivalently AA in [25]), consecutive antennas must be π phase-shifted for optimum average energy performance. Meanwhile, under other optimization criterion and/or different schemes, there is no need of carrying out any preventive phase shifting;
 - Our numerical results corroborate that correlation is beneficial under AA – SS, specially under poor LOS where channels are more random. A very counter-intuitive result is that a greater LOS and/or number of antennas is not always beneficial when transmitting the same signal simultaneously through all antennas. Meanwhile, since correlation (LOS and number of antennas) is well-known to decrease (increase) the diversity, AA – IS and SA schemes are affected by (benefited from) an increasing correlation (LOS factor and number of antennas).

Next, Section II presents the system model, while Section III presents and discusses the CSI-free WET strategies. Their performance under Rician fading is investigated in Sections IV and V, while Section VI presents numerical results. Finally, Section VII concludes the paper.

Notation: Boldface lowercase letters denote column vectors,

while boldface uppercase letters denote matrices. For instance, $\mathbf{x} = \{x_i\}$, where x_i is the i -th element of vector \mathbf{x} ; while $\mathbf{X} = \{X_{i,j}\}$, where $X_{i,j}$ is the i -th row j -th column element of matrix \mathbf{X} . By \mathbf{I} we denote the identity matrix, and by $\mathbf{1}$ we denote a vector of ones. Superscripts $(\cdot)^T$ and $(\cdot)^H$ denote the transpose and conjugate transpose operations, while $\det(\cdot)$ is the determinant, and by $\text{diag}(x_1, x_2, \dots, x_n)$ we denote the diagonal matrix with elements x_1, x_2, \dots, x_n . \mathcal{C} and \mathcal{R} are the set of complex and real numbers, respectively; while $\mathbf{i} = \sqrt{-1}$ is the imaginary unit. Additionally, $|\cdot|$ and $\text{mod}(a, b)$ are the absolute and modulo operations, respectively, while $\|\mathbf{x}\|$ denotes the euclidean norm of \mathbf{x} . $\mathbb{E}[\cdot]$ and $\text{var}[\cdot]$ denote expectation and variance, respectively, while $\Pr[A]$ is the probability of event A . $\mathbf{v} \sim \mathcal{N}(\boldsymbol{\mu}, \mathbf{R})$ and $\mathbf{w} \sim \mathcal{CN}(\boldsymbol{\mu}, \mathbf{R})$ are a Gaussian real random vector and a circularly-symmetric Gaussian complex random vector, respectively, with mean vector $\boldsymbol{\mu}$ and covariance matrix \mathbf{R} . Additionally, $p_Y(y)$ denotes the PDF of random variable (RV) Y , while $Z \sim \chi^2(m, n)$ is a non-central chi-squared RV with m degrees of freedom and parameter n . Then, according to [26, Eq.(2-1-125)] the first two central moments are given by $\mathbb{E}[Z] = m + n$, and $\text{var}[Z] = 2(m+2n)$. Finally, $J_0(\cdot)$ denotes the Bessel function of first kind and order 0 [27, §10.2].

II. SYSTEM MODEL

Consider the scenario in which a PB equipped with M antennas powers wirelessly a large set $\{S_i\}$ of single-antenna sensor nodes located nearby. Since this work deals only with CSI-free WET schemes, and for such scenarios the characterization of one sensor is representative of the overall performance, we focus our attention to the case of a generic node S . The fading channel coefficient between the j -th PB's antenna and S is denoted as $h_j \in \mathcal{C}$, $j \in \{1, \dots, M\}$, while $\mathbf{h} \in \mathcal{C}^{M \times 1}$ is a vector with all the antennas' channel coefficients.

A. Channel model

Quasi-static channels are assumed, where the fading process is considered to be constant over the transmission of a block and independent and identically distributed (i.i.d) from block to block. Without loss of generality we set the duration of a block to 1 so the terms energy and power can be indistinctly used. Specifically, we consider channels undergoing Rician fading, which is a very general assumption that allows modeling a wide variety of channels by tuning the Rician factor $\kappa \geq 0$ [26, Ch.2], e.g. when $\kappa = 0$ the channel envelope is Rayleigh distributed, while when $\kappa \rightarrow \infty$ there is a fully deterministic LOS channel. Therefore,

$$\mathbf{h} = \sqrt{\frac{\kappa}{1+\kappa}} e^{i\varphi_0} \mathbf{h}_{\text{los}} + \sqrt{\frac{1}{1+\kappa}} \mathbf{h}_{\text{nlos}} \quad (1)$$

is the normalized channel vector [28, Ch.5], where $\mathbf{h}_{\text{los}} = [1, e^{i\Phi_1}, \dots, e^{i\Phi_{M-1}}]^T$ is the deterministic LOS propagation component such that Φ_t , $t \in \{1, \dots, M-1\}$ is the mean phase shift of the $(t+1)$ -th array element with respect to the first antenna. Additionally, φ_0 accounts for an initial phase shift, while $\mathbf{h}_{\text{nlos}} \sim \mathcal{CN}(\mathbf{0}, \mathbf{R})$ represents the scattering

(Rayleigh) component. We assume a real covariance matrix $\mathbf{R} \in \mathcal{R}^{M \times M}$ for gaining in analytical tractability, which means that real and imaginary parts of \mathbf{h}_{nlos} are i.i.d and also with covariance \mathbf{R} [29]. Assume half-wavelength equally-spaced antenna elements, e.g. as in a uniform linear array (ULA), yielding

$$\Phi_t = -t\pi \sin \phi, \quad (2)$$

where $\phi \in [0, 2\pi]$ is the azimuth angle relative to the boresight of the transmitting antenna array. Such angle depends on both transmit and receive local conditions, e.g. antenna orientation, node's location, and consequently it is different for each sensor S . Additionally, let us denote by β the average RF power available at S if the PB transmits with full power over a single antenna. Under such single-antenna setup, the available RF energy at the input of the EH circuitry is given by $\beta|h_{i^*}|^2$, where i^* is the index of the active antenna. Notice that β includes the effect of both path loss and transmit power.

B. Preventive adjustment of mean phases

As mentioned earlier, ϕ and consequently Φ , are different for each sensor, which prevents us from making any preventive phase adjustment based on a specific ϕ . However, maybe we could still use the topological information embedded in (2), which tell us that Φ_t increases with t for a given ϕ , to improve the statistics of the harvested energy. To explore this, let us consider that the PB applies a preventive adjustment of the signal phase at the $(t+1)$ -th array element given by $\psi_t \in [0, 2\pi]$, while without loss of generality we set $\psi_0 = 0$. Then, the equivalent normalized channel vector seen at certain sensor S becomes $\mathbf{h}^* = \Psi \mathbf{h}$, where

$$\Psi = \text{diag}(1, e^{i\psi_1}, \dots, e^{i\psi_{M-1}}). \quad (3)$$

Now, departing from (1) we have that

$$\begin{aligned} \mathbf{h}^* &= \sqrt{\frac{\kappa}{1+\kappa}} e^{i\varphi_0} \Psi \mathbf{h}_{\text{los}} + \sqrt{\frac{1}{1+\kappa}} \Psi \mathbf{h}_{\text{nlos}} \\ &\sim \sqrt{\frac{\kappa}{1+\kappa}} e^{i\varphi_0} \left[1, e^{i(\Phi_1+\psi_1)}, \dots, e^{i(\Phi_{M-1}+\psi_{M-1})} \right]^T + \\ &\quad + \sqrt{\frac{1}{1+\kappa}} \mathcal{CN}(\mathbf{0}, \mathbf{R}), \quad (4) \end{aligned}$$

where last line comes from simple algebraic operations and using the fact that $\Psi \mathbf{h}_{\text{nlos}} \sim \mathcal{CN}(\mathbf{0}, \Psi \mathbf{R} \Psi^H) \sim \mathcal{CN}(\mathbf{0}, \mathbf{R})$ since Ψ is diagonal with unit absolute values' entries. Without loss of generality, by conveniently setting $\varphi_0 = \pi/4$ [30] so $e^{i\varphi_0} = (1 + i)/\sqrt{2}$ imposes the effect of LOS (constant) component on real and imaginary parts of the scattering (Rayleigh) component \mathbf{h}_{nlos} , we rewrite (4) as $\mathbf{h}^* = \mathbf{h}_x + i\mathbf{h}_y$, where \mathbf{h}_x and \mathbf{h}_y are independently distributed as

$$\mathbf{h}_{x,y} \sim \sqrt{\frac{1}{2(\kappa+1)}} \mathcal{N}(\sqrt{\kappa} \boldsymbol{\omega}_{x,y}, \mathbf{R}), \quad (5)$$

where $\boldsymbol{\omega}_{x,y} = [1, \cos(\Phi_1+\psi_1) \mp \sin(\Phi_1+\psi_1), \dots, \cos(\Phi_{M-1} + \psi_{M-1}) \mp \sin(\Phi_{M-1} + \psi_{M-1})]^T$.

C. EH transfer function

Finally, and after going through the channel, the RF energy is harvested at the receiver end. The EH circuitry is characterized by a non-decreasing function $g : \mathcal{R}^+ \mapsto \mathcal{R}^+$ modeling the relation between the incident and harvested RF power at S . In most of the works g is assumed to be linear for analytical tractability, e.g. [9]–[14], [16]–[23], which implies that $g(x) = \eta x$ where η is a RF-to-DC conversion efficiency constant, thus, independent of the input power. However, in practice the conversion efficiency actually depends on the input power and consequently, the relationship between the input power and the output power is nonlinear [7], [24], [25], [31]. In this work, we consider the following EH transfer function [31]

$$g(x) = g_{\max} \left(\frac{1 + e^{ab}}{1 + e^{-a(x-b)}} - 1 \right) e^{-ab}, \quad (6)$$

which is known to describe accurately the non-linearity of EH circuits by properly fitting parameters $a, b \in \mathcal{R}^+$, while g_{\max} is the harvested power at saturation.

III. CSI-FREE MULTI-ANTENNA WET STRATEGIES

Herein we overview CSI-free multiple-antenna WET strategies for an efficient wireless powering, while discussing some related practicalities.

A. All Antennas transmitting the Same Signal (AA-SS)

Under this scheme the PB transmits the same signal s simultaneously with all antennas but with equal, hence proportionally reduced, power at each. We have previously proposed such scheme in [25], where it is referred as AA, however, herein we refer to it as AA-SS to highlight explicitly its difference with respect to the AA-IS scheme (see next subsection). Under this scheme, the RF signal at the receiver side and ignoring the noise is given by $\sum_{j=1}^M \sqrt{\frac{\beta}{M}} h_j^* s$, where s is normalized such that $\mathbb{E}[s^H s] = 1$. Then, the energy harvested by S is given by

$$\xi_{\text{aa-ss}} = g(\xi_{\text{aa-ss}}^{\text{rf}}), \quad \text{where} \quad (7)$$

$$\begin{aligned} \xi_{\text{aa-ss}}^{\text{rf}} &= \mathbb{E}_s \left[\left(\sum_{j=1}^M \sqrt{\frac{\beta}{M}} h_j^* s \right)^H \left(\sum_{j=1}^M \sqrt{\frac{\beta}{M}} h_j^* s \right) \right] \\ &= \mathbb{E}_s \left[\left| \sum_{j=1}^M \sqrt{\frac{\beta}{M}} h_j^* s \right|^2 s^H s \right] \\ &= \left| \sum_{j=1}^M \sqrt{\frac{\beta}{M}} h_j^* \right|^2 \mathbb{E}[s^H s] = \frac{\beta}{M} |\mathbf{1}^T \mathbf{h}^*|^2 \quad (8) \end{aligned}$$

is the available RF energy. Notice that the terms energy and power can be used indistinctly since the block duration is normalized and the PB does not change its strategy over time.

B. All Antennas transmitting Independent Signals (AA-IS)

Instead of transmitting the same signal over all antennas, the PB may transmit power signals s_j independently generated across the antennas. This is for alleviating the issue of

destructive signal combination at s . We refer to this scheme as AA-IS, for which the RF signal at the receiver side and ignoring the noise is given by $\sum_{j=1}^M \sqrt{\frac{\beta}{M}} h_j^* s_j$, where each s_j is normalized such that $\mathbb{E}[s_j^H s_j] = 1$, $j = 1, \dots, M$. Then, the harvested energy is given by

$$\xi_{\text{aa-is}} = g(\xi_{\text{aa-is}}^{\text{rf}}), \text{ where} \quad (9)$$

$$\begin{aligned} \xi_{\text{aa-is}}^{\text{rf}} &= \mathbb{E}_s \left[\left(\sum_{j=1}^M \sqrt{\frac{\beta}{M}} h_j^* s_j \right)^H \left(\sum_{j=1}^M \sqrt{\frac{\beta}{M}} h_j^* s_j \right) \right] \\ &= \mathbb{E}_s \left[\sum_{j=1}^M \left| \sqrt{\frac{\beta}{M}} h_j^* \right|^2 s_j^H s_j \right] = \frac{\beta}{M} \sum_{j=1}^M |h_j^*|^2 \mathbb{E}[s_j^H s_j] \\ &= \frac{\beta}{M} \|\mathbf{h}^*\|^2. \end{aligned} \quad (10)$$

For both, AA-SS and AA-IS, the signal power over each antenna is $1/M$ of the total available transmit power. Additionally, notice that M RF chains are required since all the antennas are simultaneously active. This is different from the CSI-free scheme discussed next.

C. Switching Antennas (SA)

Instead of transmitting with all antennas at once, the PB may transmit the (same or different) signal s with full power by one antenna at a time such that all antennas are used during a block. This is the SA scheme we proposed in [25]. In this case just one RF chain is required, hence, reducing circuit power consumption, hardware complexity and consequently the economic cost.

Assuming equal-time allocation for each antenna, the system is equivalent to that in which each sub-block duration is $1/M$ of the total block duration, and the total harvested energy accounts for the sum of the M sub-blocks. The RF signal at the receiver side during the j -th sub-block, and ignoring the noise, is given by $\sqrt{\beta} h_j^* s$, where s is normalized such that $\mathbb{E}[s^H s] = 1$, then

$$\xi_{\text{sa}} = \frac{1}{M} \sum_{j=1}^M g(\xi_{\text{sa},j}^{\text{rf}}), \text{ where} \quad (11)$$

$$\begin{aligned} \xi_{\text{sa},j}^{\text{rf}} &= \mathbb{E}_s \left[\left(\sqrt{\beta} h_j^* s \right)^H \left(\sqrt{\beta} h_j^* s \right) \right] = \mathbb{E}_s \left[\left| \sqrt{\beta} h_j^* \right|^2 s^H s \right] \\ &= \beta |h_j^*|^2 \mathbb{E}_s [s^H s] = \beta |h_j^*|^2 \end{aligned} \quad (12)$$

is the incident RF power during the j -th sub-block.

Notice that for the simple, but commonly adopted in literature, linear EH model, both (9) and (11) match. However, in practice $g(x)$ is non-linear, and consequently (9) may differ significantly from (11). We depart from (6) to write the second derivative of $g(x)$ as

$$\frac{d^2}{dx^2} g(x) = \frac{a^2 e^{ax} (1 + e^{ab}) (e^{ab} - e^{ax}) g_{\max}}{(e^{ab} + e^{ax})^3}, \quad (13)$$

which allows us to conclude that g is convex (concave) for $x \leq b$ ($x \geq b$). Then, for certain channel vector realization \mathbf{h} and using Jensen's inequality, we have that

$$\begin{aligned} g\left(\frac{\beta}{M} \sum_{j=1}^M |h_j|^2\right) &\begin{cases} \leq \frac{1}{M} \sum_{j=1}^M g(\beta |h_j|^2), & \text{if } |h_j|^2 \leq \frac{b}{\beta} \forall j \\ \geq \frac{1}{M} \sum_{j=1}^M g(\beta |h_j|^2), & \text{if } |h_j|^2 \geq \frac{b}{\beta} \forall j \end{cases}, \\ \xi_{\text{aa-is}} &\begin{cases} \leq \xi_{\text{sa}}, & \text{if } \max |h_j|^2 \leq \frac{b}{\beta} \\ \geq \xi_{\text{sa}}, & \text{if } \min |h_j|^2 \geq \frac{b}{\beta} \end{cases}. \end{aligned} \quad (14)$$

Remark 1. Above result implies that devices far from the PB and more likely to operate near their sensitivity level, benefit more from the SA scheme than from AA-IS. However, those closer to the PB and more likely to operate near saturation, benefit more from AA-IS.

In the following we analyze the statistics of the RF energy available at S for harvesting under the AA-SS and AA-IS schemes. For such schemes, the harvested energy comes from mapping the RF energy through the EH transfer function g , as shown in (7) and (9). For SA the mapping is much more convoluted, specially because the available RF energy varies (although possibly correlationally) within the same coherence block as illustrated in (11). However, our analysis in the previous paragraphs suggests that the statistics of $\xi_{\text{aa-is}}$ and ξ_{sa} may be approximated, which is an issue we discuss numerically in detail in Section VI.

IV. RF AVAILABLE ENERGY UNDER AA-SS

Next, we characterize the distribution of the RF power at S under the AA-SS scheme.

Theorem 1. Conditioned on the mean phase shifts of the powering signals, the distribution of the RF power at the input of the energy harvester under the AA-SS operation is given by

$$\xi_{\text{aa-ss}}^{\text{rf}} \sim \frac{\beta R_{\Sigma}}{2(\kappa + 1)M} \chi^2 \left(2, \frac{2\kappa f(\boldsymbol{\psi}, \phi)}{R_{\Sigma}} \right), \quad (15)$$

where $R_{\Sigma} = \mathbf{1}^T \mathbf{R} \mathbf{1}$,

$$f(\boldsymbol{\psi}, \phi) = v_1(\boldsymbol{\psi}, \phi)^2 + v_2(\boldsymbol{\psi}, \phi)^2, \quad (16)$$

$$\begin{aligned} v_1(\boldsymbol{\psi}, \phi) &= 1 + \sum_{t=1}^{M-1} \cos(\psi_t + \Phi_t) \\ v_2(\boldsymbol{\psi}, \phi) &= \sum_{t=1}^{M-1} \sin(\psi_t + \Phi_t) \end{aligned}, \quad (17)$$

and Φ_t is given in (2) as a function of ϕ .

Proof. See Appendix A.

Notice that (15) matches [25, Eq.(25)] just in the specific case of un-shifted mean phases, e.g. $\boldsymbol{\psi} + \boldsymbol{\Phi} = \mathbf{0}$. In such case $f(\boldsymbol{\psi}, \phi)$ becomes M^2 .

A. On the impact of different phase means

The impact of different phase means on the system performance is strictly determined by $f(\boldsymbol{\psi}, \phi)$ in (15), and can be better understood by checking the main statistics, e.g. mean

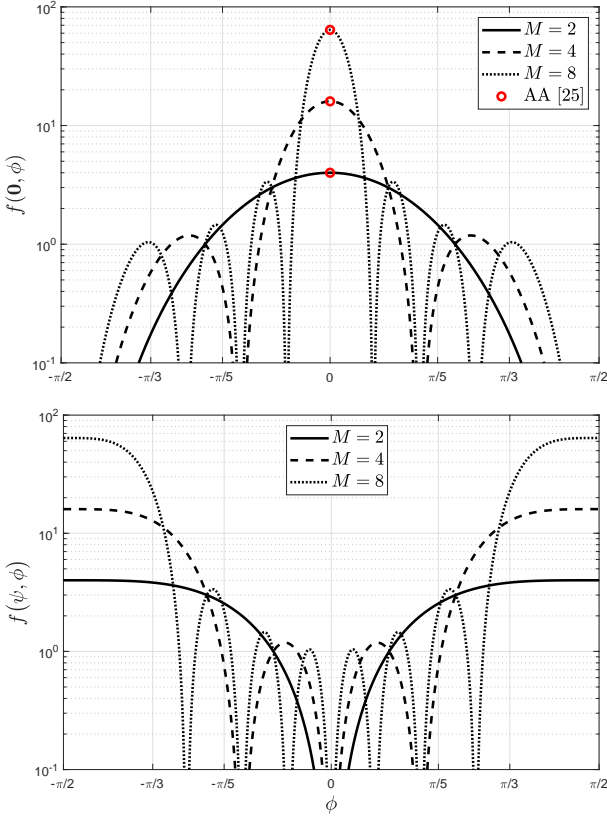


Fig. 1. a) $f(\mathbf{0}, \phi)$ vs ϕ (top), and b) $f(\boldsymbol{\psi}, \phi)$ vs ϕ for $\boldsymbol{\psi}$ according to (23) (bottom). We set $M \in \{2, 4, 8\}$.

and variance, of the incident RF power, which can be easily obtained from (15) by using as

$$\begin{aligned} \mathbb{E}[\zeta_{\text{aa-ss}}^{\text{rf}}] &= \frac{\beta R_{\Sigma}}{2(\kappa + 1)M} \left(2 + \frac{2\kappa}{R_{\Sigma}} f(\boldsymbol{\psi}, \phi) \right) \\ &= \frac{\beta}{M(\kappa + 1)} (R_{\Sigma} + \kappa f(\boldsymbol{\psi}, \phi)), \end{aligned} \quad (18)$$

$$\begin{aligned} \text{var}[\zeta_{\text{aa-ss}}^{\text{rf}}] &= \frac{\beta^2 R_{\Sigma}^2}{4(\kappa + 1)^2 M^2} \left(4 + \frac{8\kappa}{R_{\Sigma}} f(\boldsymbol{\psi}, \phi) \right) \\ &= \frac{\beta^2 R_{\Sigma}}{(\kappa + 1)^2 M^2} (R_{\Sigma} + 2\kappa f(\boldsymbol{\psi}, \phi)). \end{aligned} \quad (19)$$

Therefore, both mean and variances increases with $f(\boldsymbol{\psi}, \phi)$. Meanwhile, it is easy to check that $f(\boldsymbol{\psi}, \phi)$ is maximized for $\boldsymbol{\psi} + \boldsymbol{\Phi} = \mathbf{0}$, for which $f(\boldsymbol{\psi}, \phi) = M^2$, thus, the entire analysis carried out in [25] on this AA-SS scheme provides upper-bounds for both the mean and variance of the harvested energy. However, different phase means cause in practice a degradation on the diversity order of ξ^{rf} . Let us assume no preventive adjustment of mean phases is carried out, e.g. $\boldsymbol{\psi} = \mathbf{0}$, to illustrate in Fig. 1a the impact of such different channel phase means. Specifically, we show $f(\mathbf{0}, \phi)$ for different values of M . Notice that the performance diverges fast from the one claimed in [25] as ϕ moves away from 0.

Remark 2. *The number of minimums of $f(\boldsymbol{\psi}, \phi)$ matches M , thus, as M increases the chances of operating close to a minimum increase as well, which deteriorates significantly the system performance in terms of average incident RF power.*

B. Preventive adjustment of mean phases

Herein, we discuss on how to set the vector $\boldsymbol{\psi}$ for optimizing the system performance. For clarity, and using (17) followed by some algebraic transformations, we rewrite (16) as follows

$$\begin{aligned} f(\boldsymbol{\psi}, \phi) &= \left(1 + \sum_{t=1}^{M-1} \cos(\Phi_t + \psi_t) \right)^2 + \left(\sum_{t=1}^{M-1} \sin(\Phi_t + \psi_t) \right)^2 \\ &= M + 2 \sum_{t=1}^{M-1} \cos(\Phi_t + \psi_t) + \\ &\quad + 2 \sum_{t=1}^{M-2} \sum_{l=t+1}^{M-1} \cos(\Phi_t + \psi_t - \Phi_l - \psi_l). \end{aligned} \quad (20)$$

Assume ϕ uniformly distributed in $[0, 2\pi]^2$, e.g. $p_{\phi}(\phi) = \frac{1}{2\pi}$, then the problem translates to optimize over $f(\boldsymbol{\psi}) = \frac{1}{2\pi} \int_0^{2\pi} f(\boldsymbol{\psi}, \phi) d\phi$. Substituting (2) into (20) and integrating over ϕ we attain

$$\begin{aligned} f(\boldsymbol{\psi}) &= M + 2 \sum_{t=1}^{M-1} J_0(t\pi) \cos \psi_t + \\ &\quad + 2 \sum_{t=1}^{M-2} \sum_{l=t+1}^{M-1} J_0((t-l)\pi) \cos(\psi_t - \psi_l), \end{aligned} \quad (21)$$

which comes from using the integral representation of $J_0(\cdot)$ [27, Eq.(10.9.1)]. Obviously, (18) and (19) still hold but using $f(\boldsymbol{\psi})$ instead of $f(\boldsymbol{\psi}, \phi)$.

1) *Average energy maximization:* Solving the problem of maximizing the average incident RF power is equivalent to solve $\arg \max_{\boldsymbol{\psi}} f(\boldsymbol{\psi})$. Now, since $|\cos \alpha| \leq 1$ we have that

$$f(\boldsymbol{\psi}) \leq M + 2 \sum_{t=1}^{M-1} |J_0(t\pi)| + 2 \sum_{t=1}^{M-2} \sum_{l=t+1}^{M-1} |J_0((t-l)\pi)|. \quad (22)$$

Using the fact that $J_0(t\pi)$ is positive (negative) if t is even (odd), we can easily observe that the upper bound in (22) can be attained by setting $\psi_t = 0$ (π) for t even (odd) in (21), e.g.

$$\psi_t = \text{mod}(t, 2)\pi, \quad t \in \{0, 1, \dots, M-1\}. \quad (23)$$

Remark 3. *Above results means that consecutive antennas must be π phase-shifted for optimum average energy performance under the AA – SS scheme.*

Despite optimum $f(\boldsymbol{\psi})$ as in (22) cannot be simplified, an accurate approximation is

$$f(\boldsymbol{\psi}) \approx 0.85 \times M^{1.5}, \quad (24)$$

which comes from standard curve-fitting.

In Fig. 1b we show the impact of above preventive phase shifting on $f(\boldsymbol{\psi}, \phi)$ for different angles ϕ . By comparing Fig. 1a (no preventive phase shifting) and Fig. 1b (preventive phase shifting given in (23)), notice that *i*) the number of minimums keeps the same, *ii*) the best performance occurs now for $\phi = \pm\pi/2$, while the worst situation happens when

²This fits scenarios where the θ corresponding to each sensor is unknown, or alternatively, scenarios where there is a very large number of sensors homogeneously distributed in space such that $p_{\phi}(\phi) \approx \frac{1}{2\pi}$. Although our analysis here holds specifically for such uniform angle distribution, our procedures and ideas can be extended to other scenarios.

$\phi = 0$; and *iii*) there are considerable improvements in terms of area under the curves, which are expected to conduce to considerable improvements when averaging over ϕ .

2) *Energy dispersion minimization*: As metric of dispersion we consider the variance. Therefore, herein we aim to solve $\arg \min_{\psi} f(\psi)$; although notice that this in turns minimize the average available RF energy as well³.

Different from the maximization problem, the problem of minimizing $f(\psi)$ is not such easy to handle. We resorted to MatLab numerical solvers and realized that optimal solutions diverge significantly for different values of M . However, we found that $f(\mathbf{0})$ approximates extraordinarily to the optimum function value. Therefore, $\psi = \mathbf{0}$ *minimizes* the variance of the incident RF power, and not preventive phase shifting is required in this case. This means that

$$\begin{aligned} f(\psi) &\gtrsim f(\mathbf{0}) \\ &= M + 2 \sum_{t=1}^{M-1} J_0(t\pi) + 2 \sum_{t=1}^{M-2} \sum_{l=t+1}^{M-1} J_0((t-l)\pi) \\ &\stackrel{(a)}{\approx} 0.64 \times M, \end{aligned} \quad (25)$$

where (a) comes from standard curve-fitting.

Remark 4. Results in (24) and (25) evidence that both $\max f(\psi)$ and $\min f(\psi)$ share a polynomial dependence on M . In case of $\min f(\psi)$ such relation is linear, while $\max f(\psi)$ is roughly \sqrt{M} times greater than $\min f(\psi)$.

3) *Validation*: In Fig. 2 we show $f(\psi)$ as a function of M for i) the phase shifting in (23), which maximizes the average incident RF power, ii) $\psi = \mathbf{0}$, e.g. no preventive phase shifting, which minimizes both the variance and average statistics, and iii) the scenario discussed in [25] which is constrained to $\psi = \Phi = \mathbf{0}$. We utilized MatLab numerical optimization solvers for minimizing $f(\psi)$, but such approach was efficient just for $M \leq 32$. For greater M , MatLab solvers do not always converge and are extremely time-consuming. Meanwhile, notice that $\psi = \mathbf{0}$ indeed approaches extremely to $\arg \min_{\psi} f(\psi)$. Approximations in (24) and (25) are accurate.

4) *On the optimization gains*: By using (18), (24) and (25), the dB gain in average incident RF energy with respect to the non preventive shifting scheme, which in turns minimizes the energy dispersion according to our discussion in Subsection IV-B2, can be obtained as follows

$$\begin{aligned} \delta_{\mathbb{E}} &\approx 10 \log_{10} \left(\frac{\beta(R_{\Sigma} + 0.85\kappa M^{1.5})}{M(\kappa + 1)} \Big/ \frac{\beta(R_{\Sigma} + 0.64\kappa M)}{M(\kappa + 1)} \right) \\ &= 10 \log_{10} \left(\frac{R_{\Sigma} + 0.85\kappa M^{1.5}}{R_{\Sigma} + 0.64\kappa M} \right) \\ &\geq 10 \log_{10} \left(\frac{M + 0.85\kappa\sqrt{M}}{M + 0.64\kappa} \right), \end{aligned} \quad (26)$$

where last line comes from the fact that the argument of the logarithm is a decreasing function of R_{Σ} since $0.85\kappa M^{1.5} > 0.64\kappa M$ for $M \geq 2$, and $R_{\Sigma} \leq M^2$.

³It is easily verifiable that the phase shifting that satisfies $\arg \min_{\psi} f(\psi)$, minimizes the *coefficient of variation* parameter, which is given by $\frac{\sqrt{\text{var}[\xi]}}{\mathbb{E}[\xi]}$, and constitutes probably a more suitable dispersion metric.

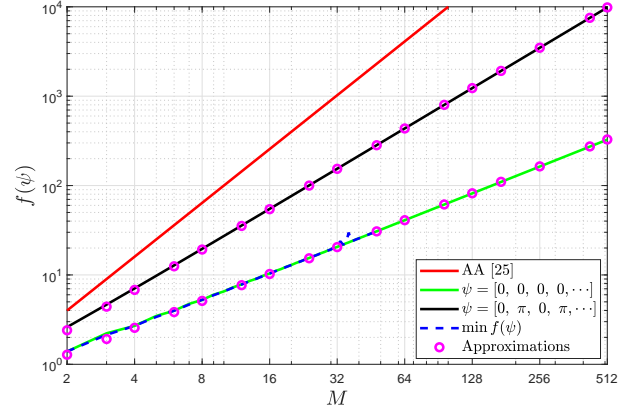


Fig. 2. $f(\psi)$ vs M .

Now, we evaluate the costs in terms of the variance increase of such average energy maximization shifting. By using (19), (24) and (25) we have that

$$\begin{aligned} \delta_{\text{var}} &\approx 10 \log_{10} \left(\frac{R_{\Sigma} + 2 \times 0.85\kappa M^{1.5}}{R_{\Sigma} + 2 \times 0.64\kappa M} \right) \\ &\stackrel{(a)}{\leq} 10 \log_{10} \left(\frac{2 \times 0.85\kappa\sqrt{M}}{2 \times 0.64\kappa} \right) \\ &= 5 \log_{10} M + 1.23, \end{aligned} \quad (27)$$

where (a) comes from using the lower-bound of R_{Σ} , e.g. $R_{\Sigma} \geq 0$. Above results imply for instance that the gain in the average incident RF energy is above 3.47 dB when $\kappa = 10$ and $M = 8$, while the variance can increase 5.75 dB maximum as well.

V. RF AVAILABLE ENERGY UNDER AA-IS

Next, we characterize the distribution of the RF power at the receiver end under the AA – IS scheme.

Theorem 2. *Conditioned on the mean phase shifts of the powering signals, the approximated distribution of the RF power available as input to the energy harvester under the AA – IS is*

$$\begin{aligned} \xi_{\text{aa-is}}^{\text{rf}} &\sim \frac{\beta}{2M^2(\kappa+1)} \left(R_{\Sigma} \chi^2 \left(2, \frac{2\kappa f(\psi, \phi)}{R_{\Sigma}} \right) + \right. \\ &\quad \left. + \frac{M^2 - R_{\Sigma}}{M-1} \chi^2 \left(2(M-1), \frac{2M(M-1)\kappa \tilde{v}(\psi, \phi)}{M^2 - R_{\Sigma}} \right) \right), \end{aligned} \quad (28)$$

where

$$\begin{aligned} \tilde{v}(\psi, \phi) &= M-1 + 2 \sum_{j=1}^{M-1} \frac{1}{j(j+1)} \left(\sum_{t=M-j+1}^{M-1} \cos(\psi_t + \Phi_t) + \right. \\ &\quad \left. + \sum_{t=M-j+1}^{M-1} \sum_{l=t+1}^{M-1} \cos(\psi_t + \Phi_t - \psi_l - \Phi_l) - j \cos(\psi_{M-j} + \Phi_{M-j}) + \right. \\ &\quad \left. - j \sum_{t=M-j+1}^{M-1} \cos(\psi_{M-j} + \Phi_{M-j} - \psi_t - \Phi_t) \right). \end{aligned} \quad (29)$$

Proof. See Appendix B.

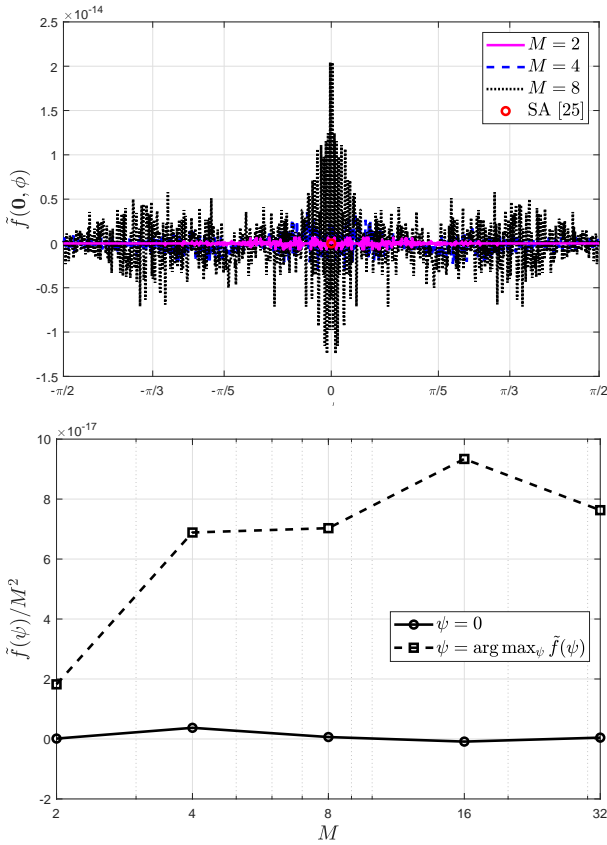


Fig. 3. a) $\tilde{f}(\mathbf{0}, \phi)$ vs ϕ for $M \in \{2, 4, 8\}$ (top), and b) $\tilde{f}(\boldsymbol{\psi})$ vs M for $\boldsymbol{\psi} = \mathbf{0}$ and $\boldsymbol{\psi} = \arg \max_{\boldsymbol{\psi}} \tilde{f}(\boldsymbol{\psi})$ (bottom).

For $\boldsymbol{\psi} + \boldsymbol{\Phi} = \mathbf{0}$, (28) matches [25, Eq.(39)]⁴. However, when mean phase shifts between antenna elements increase, both expressions diverge.

A. On the impact of different mean phases

It is not completely clear from (28) whether phase shifts are advantageous or not under this scheme. Let us start by checking the average statistics of $\zeta_{\text{aa-is}}^{\text{rf}}$ as follows

$$\begin{aligned} \mathbb{E}[\zeta_{\text{aa-is}}^{\text{rf}}] &\approx \frac{\beta}{2M^2(\kappa+1)} \left(\frac{M^2 - R_{\Sigma}}{M-1} \left(2(M-1) + \right. \right. \\ &\quad \left. \left. + \frac{2M(M-1)\kappa\tilde{v}(\boldsymbol{\psi}, \phi)}{M^2 - R_{\Sigma}} \right) + R_{\Sigma} \left(2 + \frac{2\kappa f(\boldsymbol{\psi}, \phi)}{R_{\Sigma}} \right) \right) \\ &= \frac{\beta}{M^2(\kappa+1)} \left(M^2 - R_{\Sigma} + M\kappa\tilde{v}(\boldsymbol{\psi}, \phi) + \right. \\ &\quad \left. + R_{\Sigma} + \kappa f(\boldsymbol{\psi}, \phi) \right) \\ &= \beta \left(1 + \frac{\kappa \tilde{f}(\boldsymbol{\psi}, \phi)}{M^2(\kappa+1)} \right), \end{aligned} \quad (30)$$

where $\tilde{f}(\boldsymbol{\psi}, \phi) = f(\boldsymbol{\psi}, \phi) + M\tilde{v}(\boldsymbol{\psi}, \phi) - M^2$. Notice that the larger $\tilde{f}(\boldsymbol{\psi}, \phi)$, the greater $\mathbb{E}[\zeta_{\text{aa-is}}^{\text{rf}}]$. However, $\tilde{f}(\boldsymbol{\psi}, \phi) \ll 1$

⁴Notice that [25, Eq.(39)] describes the distribution of the RF incident power under un-shifted mean phases and the SA operation considering the whole block time. Therefore, both (28) and [25, Eq.(39)] must match when $\boldsymbol{\Phi} = \mathbf{0}$ according to our discussions in Subsection III-C.

independently of the value of ϕ as shown in Fig. 3a for the case where no preventive adjustment of mean phases is carried out, e.g. $\boldsymbol{\psi} = \mathbf{0}$.

Remark 5. Therefore, channel mean phase shifts do not strictly bias the average harvested energy, which is intuitively expected since transmitted signals are independent to each other. Meanwhile, such result is very different from what happened under the AA – SS scheme for which mean phase shifts always influenced (negatively) on such metric.

Additionally, notice that when R_{Σ} is maximum (perfect correlation), AA – SS could provide up to M times more energy on average than AA – IS, whose average statistics are not affected in any way by R_{Σ} . Previous statement holds as long as there is not a strong LOS component; however, as κ takes greater values, which is typical of WET systems due to the short range characteristics, $f(\boldsymbol{\psi}, \phi)$ and $\tilde{f}(\boldsymbol{\psi}, \phi)$ become more relevant, which favors the AA – IS scheme.

Let us investigate now the impact on the variance as follows

$$\begin{aligned} \text{var}[\zeta_{\text{aa-is}}^{\text{rf}}] &\approx \frac{\beta^2}{2M^4(\kappa+1)^2} \left(\frac{(M^2 - R_{\Sigma})^2}{(M-1)^2} \left(2(M-1) + \right. \right. \\ &\quad \left. \left. + \frac{4M(M-1)\kappa\tilde{v}(\boldsymbol{\psi}, \phi)}{M^2 - R_{\Sigma}} \right) + R_{\Sigma}^2 \left(2 + \frac{4\kappa f(\boldsymbol{\psi}, \phi)}{R_{\Sigma}} \right) \right) \\ &\approx \frac{\beta^2}{M^3(M-1)(\kappa+1)^2} \left(M^3(1+2\kappa) + R_{\Sigma}^2 + \right. \\ &\quad \left. - 2MR_{\Sigma}(1+\kappa) + 2\kappa M(R_{\Sigma} - M)f(\boldsymbol{\psi}, \phi) \right), \end{aligned} \quad (31)$$

where last line comes from taking advantage of $f(\boldsymbol{\psi}, \phi) + M\tilde{v}(\boldsymbol{\psi}, \phi) - M^2 \approx 0 \rightarrow \tilde{v}(\boldsymbol{\psi}, \phi) \approx M - f(\boldsymbol{\psi}, \phi)/M$ to write $\text{var}[\zeta_{\text{aa-is}}^{\text{rf}}]$ just as a function of $f(\boldsymbol{\psi}, \phi)$. Since $f(\boldsymbol{\psi}, \phi) \geq 0$, it is obvious that just when $M > R_{\Sigma}$, e.g. negative correlation of some antennas, the system performance benefits from having different mean phases.

B. Preventive adjustment of mean phases

Herein, we discuss on how to set the vector $\boldsymbol{\psi}$ for optimizing the system performance. Again, ϕ is taken randomly and uniformly from $[0, 2\pi]$ as in Subsection IV-B.

1) *Average energy maximization.* As shown in Fig. 3a, channel mean phase shifts do not impact significantly on the average incident RF power. Then, it is intuitively expected that none preventive phase shifting would improve such average statistics. To corroborate this we require computing

$$\tilde{f}(\boldsymbol{\psi}) = \frac{1}{2\pi} \int_0^{2\pi} \tilde{f}(\boldsymbol{\psi}, \phi) d\phi,$$

for which

$$\begin{aligned}
\tilde{f}(\boldsymbol{\psi}) &= \frac{1}{2\pi} \int_0^{2\pi} f(\boldsymbol{\psi}, \phi) d\phi + \frac{M}{2\pi} \int_0^{2\pi} \tilde{v}(\boldsymbol{\psi}, \phi) d\phi - \frac{M^2}{2\pi} \int_0^{2\pi} d\phi \\
&= f(\boldsymbol{\psi}) - M + \sum_{j=1}^{M-1} \frac{4\pi}{j(j+1)} \left(\sum_{t=M-j+1}^{M-1} J_0(t\pi) \cos \psi_t + \right. \\
&\quad + \sum_{t=M-j+1}^{M-1} \sum_{l=t+1}^{M-1} J_0((l-t)\pi) \cos(\psi_t - \psi_l) + \\
&\quad - j \sum_{t=M-j+1}^{M-1} J_0((t-M+j)\pi) \cos(\psi_{M-j} - \psi_t) + \\
&\quad \left. - j J_0((M-j)\pi) \cos \psi_{M-j} \right), \quad (32)
\end{aligned}$$

where $f(\boldsymbol{\psi})$ is given in (21) and last line comes from integrating $\tilde{v}(\boldsymbol{\psi}, \phi)$ over ϕ by using the integral representation of $J_0(\cdot)$ [27, Eq.(10.9.1)]. Due to the extreme non-linearity of (32) we resort to exhaustive search optimization solvers of MatLab to find $\arg \max_{\boldsymbol{\psi}} \tilde{f}(\boldsymbol{\psi})$ and compare its performance with the non preventive phase shifting scheme for which $\boldsymbol{\psi} = \mathbf{0}$. Specifically, we show in Fig. 3b their associated performance in terms of $\tilde{f}(\boldsymbol{\psi})$ normalized by M^2 since the average incident RF power depends strictly on such ratio. Results evidence that although the performance gap is large in relative terms, it is not in absolute values. That is, not even the optimum preventive phase shifting allows increasing $\tilde{f}(\boldsymbol{\psi})/M^2$ significantly, e.g. $\tilde{f}(\boldsymbol{\psi})/M^2 \approx 0$.

Remark 6. Then, and based on (30), the average incident RF power is approximately β . Therefore, this scheme cannot take advantage of the multiple antennas to improve the average statistics of the incident RF power in any way.

2) *Energy dispersion minimization:* As in Subsection IV-B2 we consider the variance of the incident RF power as the dispersion measure. Then, we have that

$$\begin{aligned}
&\arg \min_{\boldsymbol{\psi}} \text{var}[\xi_{\text{aa-is}}^{\text{rf}}] \\
&= \begin{cases} \arg \min_{\boldsymbol{\psi}} f(\boldsymbol{\psi}), & \text{if } R_{\Sigma} > M \\ \arg \max_{\boldsymbol{\psi}} f(\boldsymbol{\psi}), & \text{if } R_{\Sigma} < M \end{cases} \\
&= \begin{cases} \boldsymbol{\psi} \approx \mathbf{0}, & \text{if } R_{\Sigma} > M \\ \psi_t = \text{mod}(t, 2)\pi, & \text{if } R_{\Sigma} < M \end{cases}, \quad (33)
\end{aligned}$$

where last line comes from using directly our previous results in Subsection IV-B.

Remark 7. Since the average incident RF energy is not affected by any phase shifting, we can conclude that (33) provides the optimum preventive phase shifting. This means that phase shifting is not required when $R_{\Sigma} > M$, as in most of the practical systems.

On the other hand, observe from (31) that the variance decreases with M , thus, although the AA – IS is not more advantageous than single antenna transmissions in terms of the provided average RF energy, it benefits significantly from the multiple antennas to reduce the energy dispersion.

TABLE I
CSI-FREE SCHEMES AND CORRESPONDING PREVENTIVE PHASE SHIFTING

Schemes	ψ_t
AA – SS _{max E}	$\text{mod}(t, 2)\pi$
AA – SS _{min var}	0
AA – IS	0
SA	0
"scheme" ($\phi = 0$) [25] (unrealistic)	0 ($\phi = 0$)

Finally, based on Subsection III-C it is expected that the phase shifting given in (33) approaches the optimum for the SA scheme as well, hence we adopt it in such scenario.

VI. NUMERICAL RESULTS

Herein we present simulation results on the performance of the discussed CSI-free multiple-antenna schemes under the non-linear EH model given in (6) with $g_{\text{max}} = 84 \mu\text{W}$ (-10.76 dBm), $a = 0.015$ and $b = 140$. We evaluate the average harvested energy, and energy outage probability, which refers to the probability that the RF energy falls below an energy threshold $\xi_0 = -16 \text{ dBm}$, thus, disabling the EH process⁵. Notice the energy outage probability is highly related with both mean and variance statistics. The EH hardware parameters were already utilized in [25] and agree with the EH circuitry experimental data in [32].

We take ϕ uniformly and randomly from $[0, 2\pi]$, while comparing the corresponding results to those with equal mean phases, $\phi = 0$, which are not attainable in practice and are just presented as benchmark. For clarity we summarize the schemes under consideration in Table I. Notice that in case of AA – IS and SA we just consider the preventive phase shifting given in the first line of (33) since we assume positive spatial correlation, e.g. $R_{\Sigma} \geq M$. Specifically, we assume exponential spatial correlation with coefficient τ such that $R_{i,j} = \tau^{|i-j|}$, hence,

$$R_{\Sigma} = M + 2 \sum_{i=1}^{M-1} (M-i)\tau^i = \frac{M(1-\tau^2) - 2\tau(1-\tau^M)}{(1-\tau)^2}, \quad (34)$$

where last step comes from using a geometric series compact representation. Such model is physically reasonable since correlation decreases with increasing distance between antennas. Unless stated otherwise we set $\kappa = 5$ and $\tau = 0.3$ to account for certain LOS and correlation, while we assume the PB is equipped with a moderate-to-small number of antennas $M = 8$.

A. On the distribution of the harvested energy

In Fig. 4 we illustrate the PDF of the energy harvested under each of the schemes. Specifically, Fig. 4a shows the PDF for two different path-loss profiles, while considering AA – IS and SA schemes. We observe that under SA the harvested energy under large path loss presents slightly better statistics than under AA – IS, while AA – IS is superior when operating under better average channel statistics. Therefore, we corroborate our statements in Remark 1: devices far from the

⁵ ξ_0 must be obviously not smaller than the EH sensitivity.

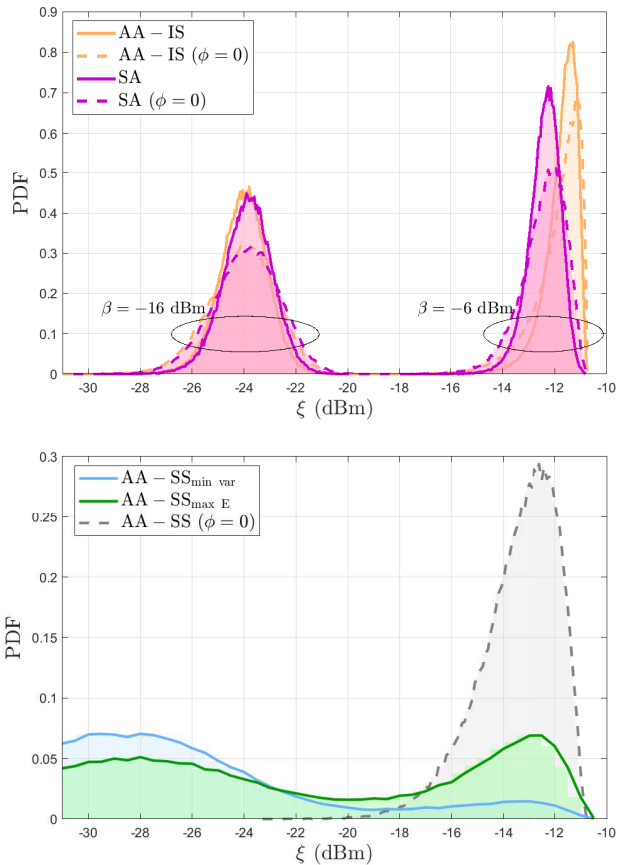


Fig. 4. PDF of the harvested energy *a*) under AA-IS and SA for $\beta \in \{-16, -6\}$ dBm, and *b*) under AA-SS for $\beta = -16$ dBm.

PB indeed benefit more from SA than from AA-IS, while those closer to the PB benefit more from the latter. We also show that the statistics improve by considering the channel mean phases, therefore, the performance of these schemes is better in a practical setup than the foreseen by [25]. Something different occurs under AA-SS as shown in Fig. 4b. As we discussed in Section IV, the un-shifted mean phase assumption is the most optimistic under the operation of AA-SS, and notice that the performance gains with respect to what can be attained in practice, e.g. under the AA-SS_{min var} and AA-SS_{max E} discussed in this work, are extremely notorious. Regarding AA-SS_{max E} vs AA-SS_{min var}, we can observe the performance gains in terms of average and variance of the harvested energy, respectively, of one with respect to the other. We must say that although AA-SS_{min var} provides less disperse harvested energy values, they could be extremely small compared to the ones achievable under AA-SS_{max E}.

Let us analyze now the CDF curves, which are shown in Fig. 5 for $\beta = -12$ dBm⁶. Notice that, although

⁶In this and most of the subsequent figures we adopt $\beta = -12$ dBm to illustrate the performance in the desired operation range, e.g. above/below sensitivity/saturation, since for an incident RF power of -12 dBm ($63 \mu\text{W}$) the harvested power becomes -19 dBm ($12 \mu\text{W}$).

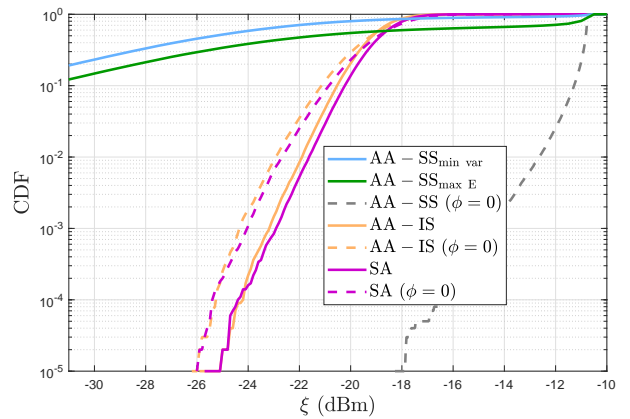


Fig. 5. CDF of the harvested energy for $\beta = -12$ dBm.

with greater variance, AA-SS_{max E} performs superior⁷ than AA-SS_{min var}. In fact, this holds in most scenarios, which highlights the need of a π -phase shifting in consecutive antennas when using the AA-SS scheme as foreseen in Remark 3. Meanwhile, the greatest diversity order is attained by AA-IS and SA schemes, which perform similarly. In this case, AA-IS performs slightly superior but this depends greatly on the path loss according to our discussions in previous paragraph. Notice that these two schemes guarantee, for instance, chances above 99% of harvesting more than -22 dBm of power, compared to just 60% and 40% when using AA-SS_{max E} and AA-SS_{min var}, respectively. Once again, the gaps with respect to the performance under un-shifted mean phases are evidenced, and are shown to be enormous specially when transmitting the same signal simultaneously by all antennas.

B. On the impact of the channel

Fig. 6 shows the average (Fig. 6a) and variance (Fig. 6b) of the harvested energy, and the energy outage probability (Fig. 6c), as a function of the path loss. In general, both the average and variance of the incident RF power increases with β for all schemes. However, the saturation phenomenon captured by (6) makes that the average harvested energy saturates at some point, while obviously the variance would decrease from that point onward. These phenomena are observed in Fig. 6a and Fig. 6b. Notice that AA-SS_{max E} achieves considerable gains in terms of average harvested energy compared to AA-SS_{min var}⁸. In fact, the performance curve of AA-SS_{max E} lies approximately in the middle between the curves of AA-SS_{min var} and the idealistic AA-SS ($\phi = 0$). Meanwhile, in terms of variance and energy outage probability they do not differ significantly. Regarding AA-IS and SA, we can observe that they even outperform AA-SS_{min var}'s performance, while AA-SS_{max E} is strictly superior in the region of large path-loss. Therefore, far devices are the most benefited from AA-SS_{max E}. Meanwhile, since the variance

⁷In this context a superior performance means that the corresponding CDF curve is below.

⁸Based on Remark 4 statement, specifically on (24) and (25), and (18), AA-SS_{max E} provides $\sim \frac{\beta\kappa}{\kappa+1} (0.85\sqrt{M} - 0.64)$ more energy units than AA-SS_{min var} on average.

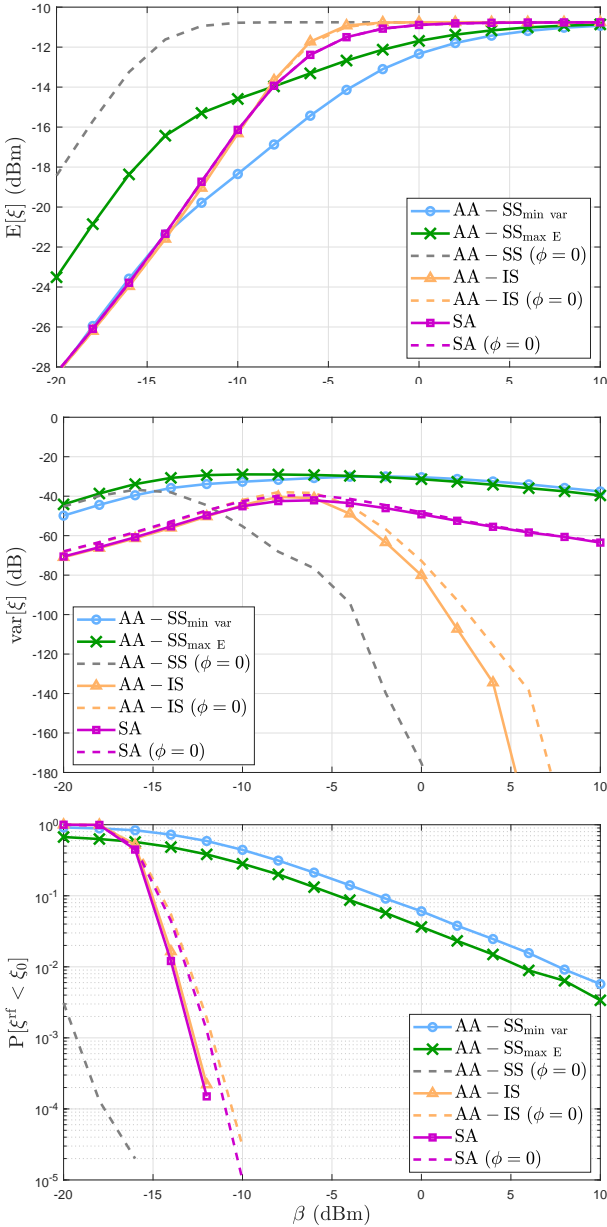


Fig. 6. *a)* Average harvested energy (top), *b)* variance of the harvested energy (middle), and *c)* energy outage probability (bottom), as a function of β .

of the incident RF energy (and also harvested energy as observed in Fig. 6b) is the lowest under AA-IS and SA, they are capable of providing a more stable energy supply, which when operating near (or in) saturation makes the devices to harvest more energy on average when compared to AA-SS_{max E}. That is why the average harvested energy under AA-IS and SA is the greatest among the practical schemes for $\beta > -8$ dBm. Specifically, AA-IS performs the best in that region, while SA is slightly better than AA-IS for $\beta < -10$ dBm. Discussions on this were carried out already in Subsections III-C and VI-A.

As we already demonstrated and verified the necessity of considering the mean phase shifts in the analysis, from now on we just focus on showing the performance results under random mean phase shifts, e.g. we dispense of “scheme” ($\phi =$

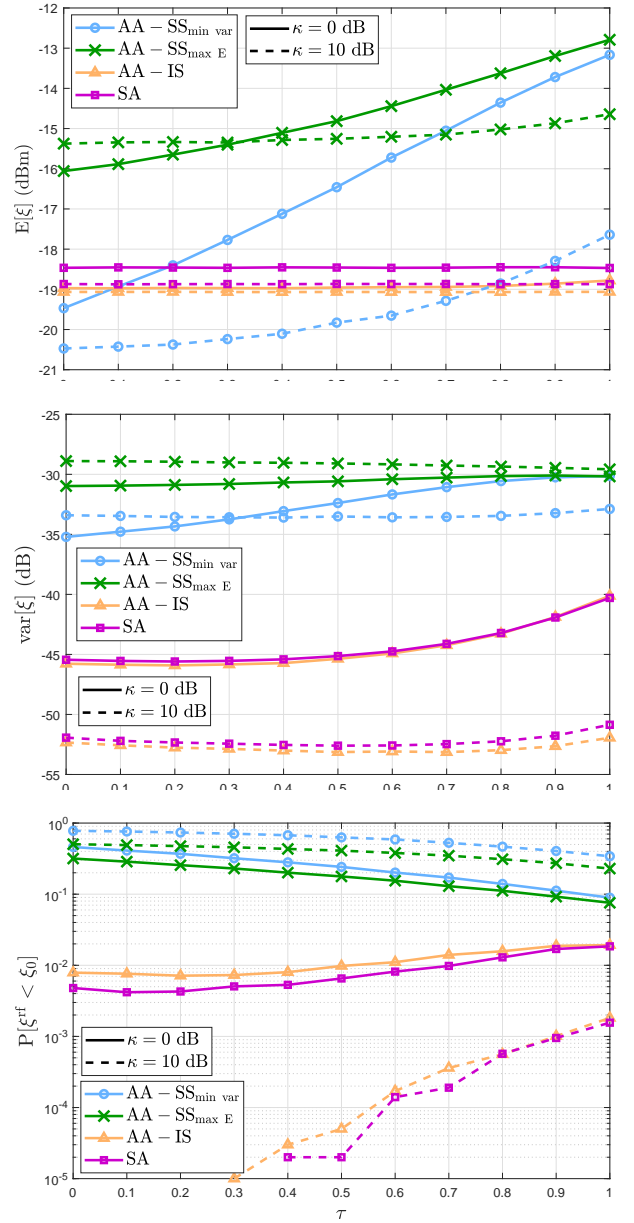


Fig. 7. *a)* Average harvested energy (top), *b)* variance of the harvested energy (middle), and *c)* energy outage probability (bottom), as a function of τ for $\kappa = \{0, 10\}$ dB and $\beta = -12$ dBm.

0) performance curves.

In Fig. 7 we show the statistics (average in Fig. 7a and variance in Fig. 7b) of the harvested energy, and the energy outage probability (Fig. 7c), as a function of the exponential correlation coefficient for two LOS profiles. As evidenced, a greater correlation is beneficial under the AA-SS schemes, specially under poor LOS where channels are more random. A very counter-intuitive result is that LOS is not always beneficial when transmitting the same signal simultaneously through all antennas. In fact, the energy outage probability under such schemes is lower for $\kappa = 0$ dB than for $\kappa = 10$ dB, which also holds in case of the average harvested energy when preventive phase shifting is not used, e.g. AA-SS_{min var}, and for $\tau > 0.35$ in case of AA-SS_{max E}. Meanwhile, since

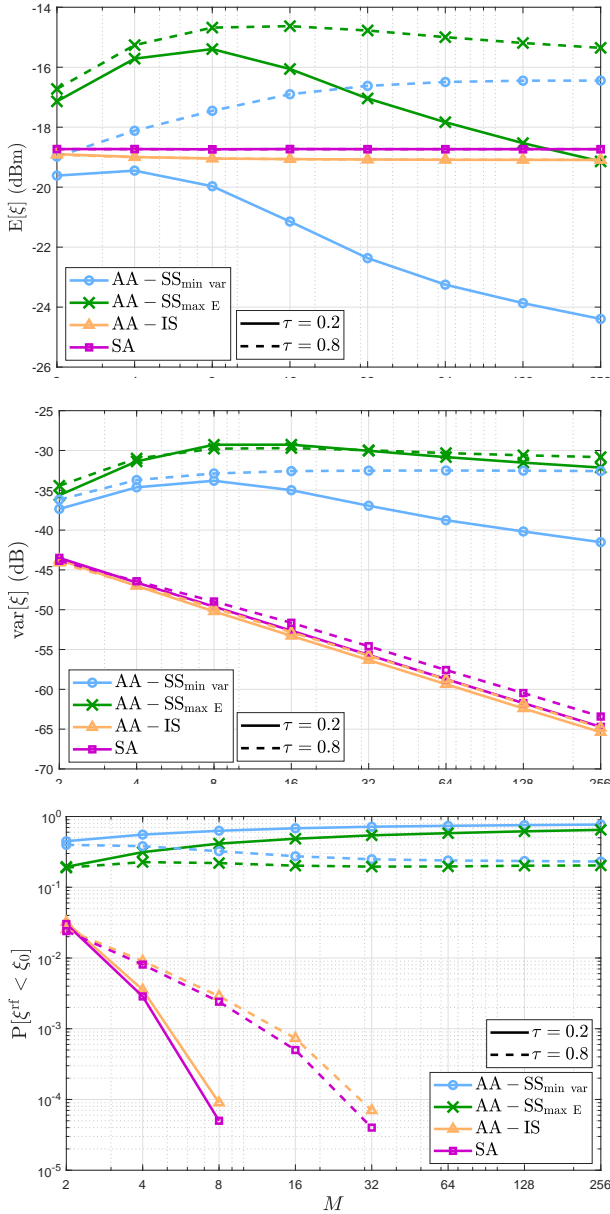


Fig. 8. *a*) Average harvested energy (top), *b*) variance of the harvested energy (middle), and *c*) energy outage probability (bottom), as a function of M for $\tau = \{0.2, 0.8\}$ and $\beta = -12$ dBm.

correlation (LOS) is well-known to decrease (increase) the diversity, AA – IS and SA schemes are affected by (benefited from) an increasing τ (κ) as shown in Fig. 7b and Fig. 7c. Notice however that as claimed in Remark 6 the average statistics of the energy harvested under such schemes is not affected in any way by the correlation, and only a bit by the LOS factor due to the non-linearity of the energy harvester. In general, AA – SS_{max E} is the clear winner in terms of maximum average harvested energy, while AA – IS and SA schemes offer better performance in terms of energy outage probability.

C. On the impact of the number of antennas

Herein we investigate the impact of the number of transmit antennas on the system performance. Fig. 8 show the average

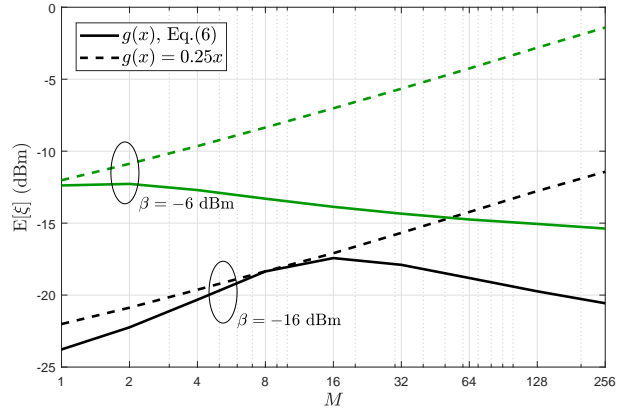


Fig. 9. Average harvested energy as a function of M for $\beta = \{-16, -6\}$ dBm. Non-linear EH model vs linear EH model with $\eta = 25\%$.

(Fig. 8a) and variance (Fig. 8b) of the harvested energy, and the energy outage probability (Fig. 8c) for $\tau = \{0.2, 0.8\}$. As expected, the average harvested energy under AA – IS and SA remains constant as M increases, while the variance and consequently the energy outage probability decrease. The latter improves as τ decreases as commented in previous subsection. Meanwhile, it is observed that a greater M not always allows improvements on the system performance when transmitting the same signal simultaneously through all antennas. Interestingly, as the correlation increases a greater number of antennas is advisable, which does not occur for small τ .

Results in Fig. 8 evidence that there is an optimum number of transmit antennas M^* . For instance, in terms of average harvested energy, $M^* = 4$ (8) and $M^* = 256$ (16) for $\tau = 0.2$ and $\tau = 0.8$, respectively, and under the operation of AA – SS_{min var} (AA – SS_{max E}). Such phenomenon is mostly due to the non-linearity of the EH circuitry. To deepen this, we show in Fig. 9 the average harvested energy as a function of M for two different path loss profiles, while comparing the performance under the non-linear EH function to the one attained under the ideal linear EH model with 25% of conversion efficiency⁹. Notice that the performance grows unbounded under such ideal model, which also happens when analyzing the average incident RF power. However, under the non-linearities of the energy harvester that is not longer the case. Since for $\beta = -6$ dBm the device is likely to be operating close to saturation, the optimum number of antennas is small, e.g. $M^* = 1$ or 2, but under greater path loss, such number goes up to $M^* = 16$.

VII. CONCLUSION

In this paper, we analyzed CSI-free schemes that a dedicated multi-antenna power station can utilize when powering wirelessly a large set of single-antenna devices. Differently from our early work [25], such CSI-free schemes were studied in a more practical setup that takes into account the mean phase shifts between antenna elements. In addition to AA – SS (All Antennas transmitting the Same Signal) and SA (Switching

⁹Instead of the maximum conversion efficiency we utilized a much more conservative value [25].

Antennas) [25] schemes, we propose and investigate the AA – IS (All Antennas transmitting Independent Signals) scheme as well. We demonstrated that those devices far from the Power Beacon (PB) and more likely to operate near their sensitivity level, benefit more from the SA scheme than from AA – IS. However, those closer to the PB and more likely to operate near saturation, benefit more from AA – IS.

We characterized the distribution of the RF energy at the EH receiver in correlated Rician fading channels under each WET scheme, and found out that while AA – IS and SA cannot take advantage of the multiple antennas to improve the average statistics of the incident RF power, the energy dispersion can be significantly reduced. Meanwhile, the gains in terms of average RF energy depend critically on the mean phase shifts between the antenna elements when using AA – SS. In that regard, we show the considerable performance gaps between the idealistic AA – SS proposed in [25] and such scheme when considering channels with different mean phases. Even under such performance degradation AA – SS still provides the greatest average RF energy when compared to AA – IS and SA, although its associated energy outage probability is generally the worst. Those trade-offs make AA – IS and SA schemes suitable for powering devices under harvest-then-transmit/cooperate-like protocols, while AA – SS seems more appropriate for scenarios where the IoT devices are allowed to accumulate energy.

Additionally, we attained the preventive phase shifting that the power station could utilize for maximizing the average energy delivery or minimizing its dispersion for each of the schemes. Specifically, consecutive antennas must be π phase-shifted for optimum average energy performance under AA – SS, while under other optimization criterion and/or different schemes, there is no need of carrying out any preventive phase shifting. Numerical results evidenced that correlation is beneficial under AA – SS, while a very counter-intuitive finding was that a greater LOS and/or number of antennas was not always beneficial under such WET scheme. Meanwhile, both AA – IS and SA schemes benefit from small correlation, and large number of antennas and LOS. All these are fundamental results that can be used when designing practical WET systems.

APPENDIX A PROOF OF THEOREM 1

Departing from (8) and using (5), the RF power available as input to the energy harvester obeys

$$\begin{aligned} \xi_{\text{aa-ss}}^{\text{rf}} &= \frac{\beta}{M} |\mathbf{1}^T \mathbf{h}_x + \mathbf{i} \mathbf{1}^T \mathbf{h}_y|^2 \\ &= \frac{\beta}{M} [(\mathbf{1}^T \mathbf{h}_x)^2 + (\mathbf{1}^T \mathbf{h}_y)^2] \\ &\stackrel{(a)}{=} \frac{\beta R_\Sigma}{2(\kappa+1)M} (\theta_x^2 + \theta_y^2) \\ &\stackrel{(b)}{=} \frac{\beta R_\Sigma}{2(\kappa+1)M} \chi^2 \left(2, \frac{2\kappa(v_1(\psi, \phi)^2 + v_2(\psi, \phi)^2)}{R_\Sigma} \right), \end{aligned} \quad (35)$$

where $R_\Sigma = \mathbf{1}^T \mathbf{R} \mathbf{1}$, while v_1 and v_2 are given in (17). Notice that (a) comes from setting $\theta_{x,y}^2 = \frac{2(\kappa+1)}{R_\Sigma} (\mathbf{1}^T \mathbf{h}_{x,y})^2$, where

$\theta_{x,y} \sim \mathcal{N}\left(\sqrt{\frac{\kappa}{R_\Sigma}}(v_1 \pm v_2), 1\right)$ since $\mathbf{1}^T \mathbf{h}_{x,y}$ is still a Gaussian RV, where the mean is equal to the sum of the means of each element of vector $\mathbf{h}_{x,y}$, while the variance equals the sum of the elements of covariance matrix $\frac{1}{2(\kappa+1)} \mathbf{R}$ [33]. Therefore, the mean and variances are $\sqrt{\frac{\kappa}{2(\kappa+1)}}(v_1 \mp v_2)$ and $\frac{R_\Sigma}{2(\kappa+1)}$, respectively. Then, (b) comes from using the definition of a non-central chi-squared RV [26, Cap.2] along with simple algebraic transformations. Finally, after using (16) we attain (15). \square

APPENDIX B PROOF OF THEOREM 2

Based on (10), the RF energy available at S under the AA – IS operation is given by

$$\xi_{\text{aa-is}}^{\text{rf}} = \frac{\beta}{M} (\mathbf{h}_x^T \mathbf{h}_x + \mathbf{h}_y^T \mathbf{h}_y), \quad (36)$$

for which we analyze its distribution as follows. Let us define $\mathbf{z}_{x,y} = \sqrt{2(\kappa+1)} \mathbf{R}^{-1/2} (\mathbf{h}_{x,y} - \sqrt{\frac{\kappa}{2(\kappa+1)}} \boldsymbol{\omega}_{x,y})$ which is distributed as $\mathcal{N}(\mathbf{0}, \mathbf{I})$, then

$$\mathbf{h}_{x,y} = \frac{1}{\sqrt{2(\kappa+1)}} \mathbf{R}^{1/2} \mathbf{z}_{x,y} + \sqrt{\frac{\kappa}{2(\kappa+1)}} \boldsymbol{\omega}_{x,y} \quad (37)$$

$$\begin{aligned} \mathbf{h}_{x,y}^T \mathbf{h}_{x,y} &= \frac{1}{2(\kappa+1)} (\mathbf{R}^{1/2} \mathbf{z}_{x,y} + \sqrt{\kappa} \boldsymbol{\omega}_{x,y})^T (\mathbf{R}^{1/2} \mathbf{z}_{x,y} + \sqrt{\kappa} \boldsymbol{\omega}_{x,y}) \\ &= \frac{1}{2(\kappa+1)} (\mathbf{z}_{x,y} + \mathbf{R}^{-1/2} \sqrt{\kappa} \boldsymbol{\omega}_{x,y})^T \mathbf{R} (\mathbf{z}_{x,y} + \mathbf{R}^{-1/2} \sqrt{\kappa} \boldsymbol{\omega}_{x,y}), \end{aligned} \quad (38)$$

where last step comes from simple algebraic transformations. Notice that $\mathbf{R} = \mathbf{Q} \boldsymbol{\Lambda} \mathbf{Q}^T$ is the spectral decomposition of \mathbf{R} [34, Ch.21], where $\boldsymbol{\Lambda}$ is a diagonal matrix containing the eigenvalues of \mathbf{R} , and \mathbf{Q} is a matrix whose column vectors are the orthogonalized eigenvectors of \mathbf{R} . In order to find the eigenvalues, $\{\lambda_j\}$, of \mathbf{R} , we require solving $\det(\mathbf{R} - \lambda \mathbf{I}) = 0$ for λ , which is analytical intractable for a general matrix \mathbf{R} . However, there is analytical tractability for the special case of uniform spatial correlation. Notice that for the special case of uniformly spatial correlated fading such that the antenna elements are correlated between each other with coefficient ρ ($R_{i,j} = \rho, \forall i \neq j$), we have that

$$R_\Sigma = M(1 + (M-1)\rho). \quad (39)$$

Also, in order to guarantee that \mathbf{R} is positive semidefinite and consequently a viable covariance matrix, ρ is lower bounded by $-\frac{1}{M-1}$ [35], thus $-\frac{1}{M-1} \leq \rho \leq 1$ and $0 \leq R_\Sigma \leq M^2$. Then, under such correlation model we have that [25, Eq.(32)]

$$\boldsymbol{\Lambda} = \text{diag}(1 - \rho, \dots, 1 - \rho, 1 + (M-1)\rho), \quad (40)$$

thus, matrix \mathbf{R} is characterized by two different eigenvalues: $1 - \rho$, which is independent of the number of antennas but has multiplicity $M - 1$, and $1 + (M - 1)\rho$, whose multiplicity is 1 but increases linearly with M . Then, matrix \mathbf{Q}^T can be written as shown at the top of the next page. Such representation can

$$\mathbf{Q}^T = \begin{bmatrix} -\frac{1}{\sqrt{1 \times 2}} & 0 & 0 & \dots & 0 & 0 & 0 & \frac{1}{\sqrt{1 \times 2}} \\ -\frac{1}{\sqrt{2 \times 3}} & 0 & 0 & \dots & 0 & 0 & \frac{2}{\sqrt{2 \times 3}} & -\frac{1}{\sqrt{2 \times 3}} \\ -\frac{1}{\sqrt{3 \times 4}} & 0 & 0 & \dots & 0 & \frac{3}{\sqrt{3 \times 4}} & -\frac{1}{\sqrt{3 \times 4}} & -\frac{1}{\sqrt{3 \times 4}} \\ -\frac{1}{\sqrt{4 \times 5}} & 0 & 0 & \dots & \frac{4}{\sqrt{4 \times 5}} & -\frac{1}{\sqrt{4 \times 5}} & -\frac{1}{\sqrt{4 \times 4}} & -\frac{1}{\sqrt{4 \times 5}} \\ \vdots & \vdots & \vdots & \ddots & \vdots & \vdots & \vdots & \vdots \\ -\frac{1}{\sqrt{(M-2)(M-1)}} & 0 & \frac{M-2}{\sqrt{(M-2)(M-1)}} & \dots & -\frac{1}{\sqrt{(M-2)(M-1)}} & -\frac{1}{\sqrt{(M-2)(M-1)}} & -\frac{1}{\sqrt{(M-2)(M-1)}} & -\frac{1}{\sqrt{(M-2)(M-1)}} \\ -\frac{1}{\sqrt{(M-1)M}} & \frac{M-1}{\sqrt{(M-1)M}} & -\frac{1}{\sqrt{(M-1)M}} & \dots & -\frac{1}{\sqrt{(M-1)M}} & -\frac{1}{\sqrt{(M-1)M}} & -\frac{1}{\sqrt{(M-1)M}} & -\frac{1}{\sqrt{(M-1)M}} \\ \frac{1}{\sqrt{M}} & \frac{1}{\sqrt{M}} & \frac{1}{\sqrt{M}} & \dots & \frac{1}{\sqrt{M}} & \frac{1}{\sqrt{M}} & \frac{1}{\sqrt{M}} & \frac{1}{\sqrt{M}} \end{bmatrix}. \quad (41)$$

be verified for any M by using specialized software for matrix processing such as MatLab or Wolfram.

Now, by substituting $\mathbf{R} = \mathbf{Q}\mathbf{\Lambda}\mathbf{Q}^T$ into (38) while setting $\zeta_{x,y} = 2(\kappa+1)\mathbf{h}_{x,y}^T \mathbf{h}_{x,y}$ yields

$$\begin{aligned} \zeta_{x,y} &= \left(\mathbf{z}_{x,y} + \sqrt{\kappa}(\mathbf{Q}\mathbf{\Lambda}\mathbf{Q}^T)^{-\frac{1}{2}} \boldsymbol{\omega}_{x,y} \right)^T \mathbf{Q}\mathbf{\Lambda}\mathbf{Q}^T \times \\ &\quad \times \left(\mathbf{z}_{x,y} + \sqrt{\kappa}(\mathbf{Q}\mathbf{\Lambda}\mathbf{Q}^T)^{-\frac{1}{2}} \boldsymbol{\omega}_{x,y} \right) \\ &\stackrel{(a)}{=} \left(\mathbf{Q}^T \mathbf{z}_{x,y} + \sqrt{\kappa} \boldsymbol{\Lambda}^{-\frac{1}{2}} \mathbf{Q}^T \boldsymbol{\omega}_{x,y} \right)^T \boldsymbol{\Lambda} \times \\ &\quad \times \left(\mathbf{Q}^T \mathbf{z}_{x,y} + \sqrt{\kappa} \boldsymbol{\Lambda}^{-\frac{1}{2}} \mathbf{Q}^T \boldsymbol{\omega}_{x,y} \right) \\ &\stackrel{(b)}{=} \left(\mathbf{P}_{x,y} + \sqrt{\kappa} \mathbf{u}_{x,y} \right)^T \boldsymbol{\Lambda} \left(\mathbf{P}_{x,y} + \sqrt{\kappa} \mathbf{u}_{x,y} \right) \\ &\stackrel{(c)}{=} \sum_{j=1}^M \lambda_j \left(c_j + \sqrt{\kappa} u_{x,y_j} \right)^2, \end{aligned} \quad (42)$$

where (a) comes after some algebraic transformations, (b) follows from taking $\mathbf{P}_{x,y} = \mathbf{Q}^T \mathbf{z}_{x,y} \sim \mathcal{N}(\mathbf{0}, \mathbf{I})$ and

$$\begin{aligned} \mathbf{u}_{x,y} &= \boldsymbol{\Lambda}^{-\frac{1}{2}} \mathbf{Q}^T \boldsymbol{\omega}_{x,y} \\ &= \boldsymbol{\Lambda}^{-\frac{1}{2}} \begin{bmatrix} \frac{1}{\sqrt{2}} (\omega_M - \omega_1) \\ \frac{1}{\sqrt{2 \times 3}} (2\omega_{M-1} - \omega_1 - \omega_M) \\ \frac{1}{\sqrt{3 \times 4}} (3\omega_{M-2} - \omega_1 - \sum_{j=M-1}^M \omega_j) \\ \frac{1}{\sqrt{4 \times 5}} (4\omega_{M-3} - \omega_1 - \sum_{j=M-2}^M \omega_j) \\ \vdots \\ \frac{1}{\sqrt{(M-2)(M-1)}} ((M-2)\omega_3 - \omega_1 - \sum_{j=4}^M \omega_j) \\ \frac{1}{\sqrt{(M-1)M}} ((M-1)\omega_2 - \omega_1 - \sum_{j=3}^M \omega_j) \\ \frac{1}{\sqrt{M}} \sum_{j=1}^M \omega_j \end{bmatrix}, \end{aligned} \quad (43)$$

$$u_{x,y_j} = \begin{cases} \frac{j\omega_{M-j+1} - \omega_1 - \sum_{t=M-j+2}^M \omega_t}{\sqrt{j(j+1)}\lambda_j}, & \text{for } j \leq M-1 \\ \frac{1}{\sqrt{M}\lambda_M} \sum_{t=1}^M \omega_t, & \text{for } j = M \end{cases}, \quad (44)$$

which come from using (40) and (41); while (c) follows after taking $c_j \sim \mathcal{N}(0, 1)$.

By incorporating these results into (36) we obtain the

distribution of $\xi_{\text{aa-is}}^{\text{rf}}$ as follows

$$\begin{aligned} \xi_{\text{aa-is}}^{\text{rf}} &\sim \frac{\beta}{2M(\kappa+1)} (\zeta_x + \zeta_y) \\ &\sim \frac{\beta}{2M(\kappa+1)} \sum_{j=1}^M \lambda_j \left((c_j + \sqrt{\kappa} u_{x_j})^2 + (\tilde{c}_j + \sqrt{\kappa} u_{y_j})^2 \right) \\ &\sim \frac{\beta}{2M(\kappa+1)} \left((1-\rho)\chi^2 \left(2(M-1), \frac{2\kappa\tilde{v}(\boldsymbol{\psi}, \boldsymbol{\phi})}{1-\rho} \right) + \right. \\ &\quad \left. + (1+(M-1)\rho)\chi^2 \left(2, \frac{\kappa f(\boldsymbol{\psi}, \boldsymbol{\phi})}{M(1+(M-1)\rho)} \right) \right) \end{aligned} \quad (45)$$

since $\tilde{c}_j \sim \mathcal{N}(0, 1)$,

$$\begin{aligned} u_{x_M}^2 + u_{y_M}^2 &= \frac{1}{M\lambda_M} \left(\left(\sum_{t=1}^M \omega_{x_t} \right)^2 + \left(\sum_{t=1}^M \omega_{y_t} \right)^2 \right) \\ &= \frac{(v_1(\boldsymbol{\psi}, \boldsymbol{\phi}) - v_2(\boldsymbol{\psi}, \boldsymbol{\phi}))^2 + (v_1(\boldsymbol{\psi}, \boldsymbol{\phi}) + v_2(\boldsymbol{\psi}, \boldsymbol{\phi}))^2}{M(1+(M-1)\rho)} \\ &= \frac{2f(\boldsymbol{\psi}, \boldsymbol{\phi})}{M(1+(M-1)\rho)}, \end{aligned} \quad (46)$$

while $\tilde{v} = \frac{1}{2} \sum_{j=1}^{M-1} \lambda_j (u_{x_j}^2 + u_{y_j}^2)$, which appears expanded as a function of $\boldsymbol{\psi}$ and $\boldsymbol{\Phi}$ in (29) at the top of the next page (below (41)) and it is obtained by (a) using (44), (b) expanding the quadratic binomials, and (c) performing some algebraic simplifications by taking advantage of $\sin^2 a + \cos^2 a = 1$. Then, we attain (29) by regrouping terms and performing further algebraic simplifications by taking advantage of $\cos a \cos b + \sin a \sin b = \cos(a-b)$.

Notice that (45) holds under the assumption of uniform spatial correlation; however, given that for the AA scheme we were able of writing the distribution merely as a function of parameter R_{Σ} , which is not linked to any specific kind of correlation, we can expect that the behavior under the AA-IS scheme depends, at least approximately, on R_{Σ} rather on the specific entries of matrix \mathbf{R} . In fact, such hypothesis has been shown to be accurate under the scenario of LOS components with equal mean phases studied in [25]. To explore this, we substitute $\rho = \frac{R_{\Sigma} - M}{M(M-1)}$ coming from (39), into (45), such that we attain (28). \square

A. Validation

To evaluate the accuracy of (28) we utilize the Bhattacharyya distance metric [36], which measures the similarity of two probability distributions \mathbf{p}_1 and \mathbf{p}_2 , and it is given by

$$d_B(\mathbf{p}_1, \mathbf{p}_2) = -\ln(c_B(\mathbf{p}_1, \mathbf{p}_2)), \quad (48)$$

$$\begin{aligned}
\tilde{v}(\boldsymbol{\psi}, \phi) &\stackrel{(a)}{=} \sum_{j=1}^{M-1} \frac{1}{2j(j+1)} \left(\left(j\omega_{x_{M-j+1}} - \omega_{x_1} - \sum_{t=M-j+2}^M \omega_{x_t} \right)^2 + \left(j\omega_{y_{M-j+1}} - \omega_{y_1} - \sum_{t=M-j+2}^M \omega_{y_t} \right)^2 \right) \\
&\stackrel{(b)}{=} \sum_{j=1}^{M-1} \frac{1}{2j(j+1)} \left(j^2(\omega_{x_{M-j+1}}^2 + \omega_{y_{M-j+1}}^2) + 2 + \left(\sum_{t=M-j+2}^M \omega_{x_t} \right)^2 + \left(\sum_{t=M-j+2}^M \omega_{y_t} \right)^2 - 2j(\omega_{x_{M-j+1}} + \omega_{y_{M-j+1}}) + \right. \\
&\quad \left. - 2j \left(\omega_{x_{M-j+1}} \sum_{t=M-j+2}^M \omega_{x_t} + \omega_{y_{M-j+1}} \sum_{t=M-j+2}^M \omega_{y_t} \right) + 2 \sum_{t=M-j+2}^M (\omega_{x_t} + \omega_{y_t}) \right) \\
&\stackrel{(c)}{=} \sum_{j=1}^{M-1} \frac{1}{j(j+1)} \left(\left(\sum_{t=M-j+1}^{M-1} \cos(\psi_t + \Phi_t) \right)^2 + \left(\sum_{t=M-j+1}^{M-1} \sin(\psi_t + \Phi_t) \right)^2 + j^2 + 1 - 2j \cos(\psi_{M-j} + \Phi_{M-j}) + \right. \\
&\quad \left. - 2j \left(\cos(\psi_{M-j} + \Phi_{M-j}) \sum_{t=M-j+1}^{M-1} \cos(\psi_t + \Phi_t) + \sin(\psi_{M-j} + \Phi_{M-j}) \sum_{t=M-j+1}^{M-1} \sin(\psi_t + \Phi_t) \right) + 2 \sum_{t=M-j+1}^{M-1} \cos(\psi_t + \Phi_t) \right). \quad (47)
\end{aligned}$$

where c_B is the Bhattacharyya coefficient [36]. In the case of our interest, both probability distributions characterize $\xi_{\text{aa-is}}^{\text{rf}}$; however, for \mathbf{p}_1 we assume a uniform spatial correlation matrix \mathbf{R} , thus we may use (28) which is exact in such scenario; while for \mathbf{p}_2 we assume a randomly generated correlation matrix \mathbf{R}^* such that $R_{\Sigma} = R_{\Sigma}^*$, thus, we evaluate the distribution directly from (36). We utilize the histogram formulation for estimating \mathbf{p}_1 and \mathbf{p}_2 . Specifically, we estimate $\hat{\mathbf{p}}_1 = \{\hat{p}_{1,i}\}_{i=1,\dots,m}$ (with $\sum_{i=1}^m \hat{p}_{1,i} = 1$) and $\hat{\mathbf{p}}_2 = \{\hat{p}_{2,i}\}_{i=1,\dots,m}$ (with $\sum_{i=1}^m \hat{p}_{2,i} = 1$), where m is the number of histogram bins. Then, Bhattacharyya coefficient is calculated as [36]

$$c_B(\hat{\mathbf{p}}_1, \hat{\mathbf{p}}_2) = \sum_{i=1}^m \sqrt{\hat{p}_{1,i} \hat{p}_{2,i}}. \quad (49)$$

By substituting (49) into (48) we calculate the similarity between distributions. Note that according to (28) we have that $d_B(\mathbf{p}_1, \mathbf{p}_2) \in [0, \infty)$, where 0 corresponds to the case when $\mathbf{p}_1 = \mathbf{p}_2$.

Fig. 10a shows the average Bhattacharyya distance, \bar{d}_B , as a function of κ and ϕ for $M \in \{4, 8\}$, $\boldsymbol{\psi} = \mathbf{0}$ (no preventive phase shifting) and $\boldsymbol{\psi}$ taken uniformly random from $[0, 2\pi]^{M-1}$ to account for different possible preventive phase shiftings. We generated 1000 random correlation matrices and averaged over the Bhattacharyya distance for the distributions corresponding to each of them. We utilized 2×10^5 distribution samples and set $m = 240$, while the histogram edges were uniformly chosen between 0 and 6, which is an appropriate range since, without loss of generality, we used $\beta = 1$. As observed in the figure, the largest difference between both distributions is when $\boldsymbol{\psi} = \mathbf{0}$, M is small, e.g. $M = 4$, and $\phi \approx \pi/4 \pm \pi/2$. In such scenario \bar{d}_B increases with κ ; however, according to further extensive simulations although d_B values become close to 0.012 they never surpass such limit. Meanwhile, for other parameter configurations \bar{d}_B becomes significantly smaller.

We select $\bar{d}_B = 0.010$ and $\bar{d}_B = 0.002$ to illustrate the cases of respectively large and small differences between the considered distributions in Fig. 10b. Notice that the approximate distributions indeed approach the exact ones, even with

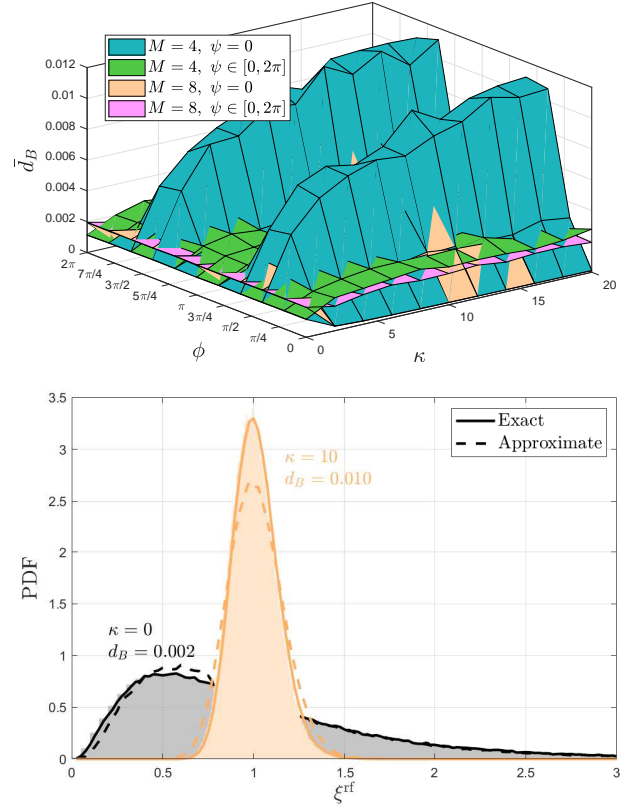


Fig. 10. a) Average Bhattacharyya distance between $\hat{\mathbf{p}}_1$ and $\hat{\mathbf{p}}_2$ as a function of κ and ϕ for $M \in \{4, 8\}$, $\boldsymbol{\psi} = \mathbf{0}$ (no preventive phase shifting) and $\boldsymbol{\psi}$ taken uniformly random from $[0, 2\pi]^{M-1}$ (top). b) Monte Carlo-based comparison between the exact \mathbf{p}_2 and proposed approximate \mathbf{p}_1 distributions of the incident RF power under the AA-IS scheme. We set $M = 4$, $\phi = 3\pi/4$ and $\boldsymbol{\psi} = \mathbf{0}$. The comparison is carried out for two different cases: i) $\kappa = 0$, $\bar{d}_B = 0.002$; and ii) $\kappa = 10$, $\bar{d}_B = 0.010$ (bottom).

greater accuracy for smaller d_B as expected. Finally, since $\bar{d}_B = 0.010$ is a very pessimistic assumption as it is only reachable for few values of ϕ , results in Fig. 10b validate the accuracy of (28) in general scenarios.

REFERENCES

- [1] M. Shirvanimoghaddam, M. Dohler, and S. J. Johnson, "Massive non-orthogonal multiple access for cellular IoT: Potentials and limitations,"

- IEEE Commun. Mag.*, vol. 55, no. 9, pp. 55–61, Sep. 2017.
- [2] O. L. A. López, H. Alves, R. D. Souza, S. Montejo-Sánchez, E. M. G. Fernández, and M. Latva-aho, “Massive wireless energy transfer: Enabling sustainable IoT towards 6G era,” *arXiv preprint arXiv:1912.05322*, 2019.
- [3] L.-G. Tran, H.-K. Cha, and W.-T. Park, “RF power harvesting: a review on designing methodologies and applications,” *Micro Nanosyst. Lett.*, vol. 5, no. 1, p. 14, Feb 2017.
- [4] H. Jayakumar, K. Lee, W. S. Lee, A. Raha, Y. Kim, and V. Raghunathan, “Powering the Internet of Things,” in *ISLPED*. New York, NY, USA: ACM, 2014, pp. 375–380.
- [5] Y. Zhang, F. Zhang, Y. Shakhsheer, J. D. Silver, A. Klinefelter, M. Nagaraju, J. Boley, J. Pandey, A. Shrivastava, E. J. Carlson, A. Wood, B. H. Calhoun, and B. P. Otis, “A batteryless 19 μ W MICS/ISM-band energy harvesting body sensor node SoC for ExG applications,” *IEEE J. Solid-State Circuits*, vol. 48, no. 1, pp. 199–213, Jan 2013.
- [6] F. Moreno-Cruz, V. T. Lopez, F. J. Romero, C. Hambeck, D. P. Morales, and A. Rivadeneyra, “Use of low-cost printed sensors with RF energy harvesting for IoT,” in *SSI*, April 2019, pp. 1–4.
- [7] B. Clerckx, R. Zhang, R. Schober, D. W. K. Ng, D. I. Kim, and H. V. Poor, “Fundamentals of wireless information and power transfer: From RF energy harvester models to signal and system designs,” *IEEE J. Sel. Areas Commun.*, vol. 37, no. 1, pp. 4–33, Jan 2019.
- [8] S. Bi, Y. Zeng, and R. Zhang, “Wireless powered communication networks: an overview,” *IEEE Wireless Commun.*, vol. 23, no. 2, pp. 10–18, April 2016.
- [9] H. Ju and R. Zhang, “Throughput maximization in wireless powered communication networks,” *IEEE Trans. Wireless Commun.*, vol. 13, no. 1, pp. 418–428, January 2014.
- [10] O. L. A. López, H. Alves, R. D. Souza, and E. M. G. Fernández, “Ultra-reliable short-packet communications with wireless energy transfer,” *IEEE Signal Process. Lett.*, vol. 24, no. 4, pp. 387–391, April 2017.
- [11] O. L. A. López, H. Alves, R. D. Souza, S. Montejo-Sánchez, and E. M. G. Fernández, “Rate control for wireless-powered communication network with reliability and delay constraints,” *IEEE Trans. Wireless Commun.*, vol. 18, no. 12, pp. 5791–5805, Dec 2019.
- [12] H. Chen, Y. Li, J. L. Rebelatto, B. F. Uchôa-Filho, and B. Vucetic, “Harvest-then-cooperate: Wireless-powered cooperative communications,” *IEEE Trans. Signal Process.*, vol. 63, no. 7, pp. 1700–1711, April 2015.
- [13] O. L. A. López, E. M. G. Fernández, R. D. Souza, and H. Alves, “Ultra-reliable cooperative short-packet communications with wireless energy transfer,” *IEEE Sensors J.*, vol. 18, no. 5, pp. 2161–2177, March 2018.
- [14] O. L. A. López, R. D. Souza, H. Alves, and E. M. G. Fernández, “Ultra reliable short message relaying with wireless power transfer,” in *IEEE ICC*, May 2017, pp. 1–6.
- [15] O. L. A. López, E. M. G. Fernández, R. D. Souza, and H. Alves, “Wireless powered communications with finite battery and finite blocklength,” *IEEE Trans. Commun.*, vol. 66, no. 4, pp. 1803–1816, April 2018.
- [16] B. T. Bacinoglu, O. Kaya, and E. Uysal-Biyikoglu, “Energy efficient transmission scheduling for channel-adaptive wireless energy transfer,” in *IEEE WCNC*, April 2018, pp. 1–6.
- [17] H. Li, K. Ota, and M. Dong, “Energy cooperation in battery-free wireless communications with radio frequency energy harvesting,” *ACM Trans. Embed. Comput. Syst.*, vol. 17, no. 2, pp. 44:1–44:17, Feb. 2018.
- [18] K. Huang and V. K. N. Lau, “Enabling wireless power transfer in cellular networks: Architecture, modeling and deployment,” *IEEE Trans. Wireless Commun.*, vol. 13, no. 2, pp. 902–912, February 2014.
- [19] W. Huang, H. Chen, Y. Li, and B. Vucetic, “On the performance of multi-antenna wireless-powered communications with energy beamforming,” *IEEE Trans. Veh. Technol.*, vol. 65, no. 3, pp. 1801–1808, March 2016.
- [20] J. Park, Y. Jeon, and S. Han, “Energy beamforming for wireless power transfer in MISO heterogeneous network with power beacon,” *IEEE Commun. Lett.*, vol. 21, no. 5, pp. 1163–1166, May 2017.
- [21] Y. Zeng and R. Zhang, “Optimized training design for wireless energy transfer,” *IEEE Trans. Commun.*, vol. 63, no. 2, pp. 536–550, Feb 2015.
- [22] —, “Optimized training for net energy maximization in multi-antenna wireless energy transfer over frequency-selective channel,” *IEEE Trans. Commun.*, vol. 63, no. 6, pp. 2360–2373, June 2015.
- [23] S. Bi and R. Zhang, “Placement optimization of energy and information access points in wireless powered communication networks,” *IEEE Trans. Wireless Commun.*, vol. 15, no. 3, pp. 2351–2364, March 2016.
- [24] Y. Chen, N. Zhao, and M. Alouini, “Wireless energy harvesting using signals from multiple fading channels,” *IEEE Trans. Commun.*, vol. 65, no. 11, pp. 5027–5039, Nov 2017.
- [25] O. L. A. López, H. Alves, R. D. Souza, and S. Montejo-Sánchez, “Statistical analysis of multiple antenna strategies for wireless energy transfer,” *IEEE Trans. Commun.*, vol. 67, no. 10, pp. 7245–7262, Oct 2019.
- [26] J. Proakis, “Digital communications,” 2001.
- [27] I. Thompson, “NIST handbook of mathematical functions,” 2011.
- [28] J. R. Hampton, *Introduction to MIMO communications*. Cambridge university press, 2013.
- [29] P. J. Schreier and L. L. Scharf, *Statistical signal processing of complex-valued data: The theory of improper and noncircular signals*. Cambridge university press, 2010.
- [30] M. A. Khalighi, J. . Brossier, G. Jourdain, and K. Raouf, “On capacity of Rician MIMO channels,” in *IEEE PIMRC*, vol. 1, Oct 2001, pp. A–A.
- [31] E. Boshkovska, D. W. K. Ng, N. Zlatanov, and R. Schober, “Practical non-linear energy harvesting model and resource allocation for SWIPT systems,” *IEEE Commun. Lett.*, vol. 19, no. 12, pp. 2082–2085, Dec 2015.
- [32] T. Le, K. Mayaram, and T. Fiez, “Efficient far-field radio frequency energy harvesting for passively powered sensor networks,” *IEEE J. Solid-State Circuits*, vol. 43, no. 5, pp. 1287–1302, May 2008.
- [33] A. Novosyolov, “The sum of dependent normal variables may be not normal,” *Institute of Computational Modelling, Siberian Branch of the Russian Academy of Sciences, Krasnoyarsk, Russia*, 2006.
- [34] D. Harville, *Matrix algebra from a statistician’s perspective*. New York: Springer-Verlag, 2008.
- [35] X. Chen, “Antenna correlation and its impact on multi-antenna system,” *PIER*, vol. 62, pp. 241–253, 2015.
- [36] T. Kailath, “The divergence and bhattacharyya distance measures in signal selection,” *IEEE Trans. Commun. Technol.*, vol. 15, no. 1, pp. 52–60, February 1967.